Millennial Recurrence of Large Earthquakes on the Haiyuan Fault near Songshan, Gansu Province, China

Jing Liu-Zeng, Yann Klinger, Xiwei Xu, Cécile Lasserre, Guihua Chen, Wenbing Chen, Paul Tapponnier, Biao Zhang

Bulletin of the Seismological Society of America, Vol. 97, No. 1B, pp. 14–34, February 2007, doi: 10.1785/0120050118

Ⓔ

Millennial Recurrence of Large Earthquakes on the Haiyuan Fault near Songshan, Gansu Province, China

by Jing Liu-Zeng, Yann Klinger, Xiwei Xu, Cécile Lasserre, Guihua Chen, Wenbing Chen, Paul Tapponnier, and Biao Zhang

Abstract The Haiyuan fault is a major active left-lateral fault along the northeast edge of the Tibet-Qinghai Plateau. Studying this fault is important in understanding current deformation of the plateau and the mechanics of continental deformation in general. Previous studies have mostly focused on the slip rate of the fault. Paleoseismic investigations on the fault are sparse, and have been targeted mostly at the stretch of the fault that ruptured in the 1920 $M \sim 8.6$ earthquake in Ningxia Province. To investigate the millennial seismic history of the western Haiyuan fault, we opened two trenches in a small pull-apart basin near Songshan, in Gansu Province. The excavation exposes sedimentary layers of alternating colors: dark brown silty to clayey deposit and light yellowish brown layers of coarser-grained sandy deposit. The main fault zone is readily recognizable by the disruption and tilting of the layers. Six paleoseismic events are identified and named SS1 through SS6, from youngest to oldest. Charcoal is abundant, yet generally tiny in the shallowest parts of the trench exposures. Thirteen samples were dated to constrain the ages of paleoseismic events. All six events have occurred during the past 3500–3900 years. The horizontal offsets associated with these events are poorly known. However, events SS3 to SS6 appear to be large ones, judging from comparison of vertical separations and widths of fault zones. The youngest event SS1 instead seems to be a minor one, probably the 1990 M_w 5.8 earthquake. Thus, four large events in 3500–3900 years would imply a recurrence interval of about 1000 years. Three events SS2 to SS4 prior to 1990 occurred sometime during 1440–1640 A.D., shortly after 890–1000 A.D. and 0–410 A.D., respectively. We tentatively associate them with the 1514 A.D., 1092 A.D., and 143 or 374 A.D. historical earthquakes. Taking 10 ± 2 m of slip for large events (SS3 and SS4), comparable to the 1920 $M > 8$ Haiyuan earthquake, their occurrence times would be consistent with the long-term 12 ± 4 mm/yr estimate of Lasserre *et al.* (1999). However, a more realistic evaluation of slip rate and its possible change with time requires a more rigorous determination of coseismic slip amounts of past earthquakes.

Online material: Trench photos with interpretation.

Introduction

The Haiyuan, Altyn Tagh, and Kunlun faults are three large, active left-lateral strike-slip faults in northern Tibet (Fig. 1a, inset). How fast these faults move is a diagnostic test of modes of deformation of the Tibet Plateau (e.g., England and Houseman, 1986; Peltzer and Tapponnier, 1988; Avouac and Tapponnier, 1993; Houseman and England, 1993; Tapponnier *et al.*, 2001). Therefore much effort has been devoted to the determination of geological slip rates during the late Pleistocene-Holocene (e.g., Zhang *et al.*, 1988; Working group on the Altyn Tagh active fault, 1992; He *et al.*, 1994, 1996; Gaudemer *et al.*, 1995; Yuan *et al.*, 1998; Lasserre *et al.*, 1999, 2002; van der Woerd *et al.*, 2000, 2002; Mériaux *et al.*, 2004, 2005) and of current Global Positioning System (GPS) geodetic rates (e.g., Bendick *et al.*, 2000; Shen *et al.*, 2001; Wang *et al.*, 2001; Chen *et al.*, 2004; Zhang *et al.*, 2004; Wallace *et al.*, 2005).

GPS-derived rates are not systematically consistent with geologic rates. For example, the 6–9 mm/yr GPS rates (Bendick *et al.*, 2000; Shen *et al.*, 2001; Zhang *et al.*, 2004; Wallace *et al.*, 2005) and the 18–27 mm/yr geologic rates

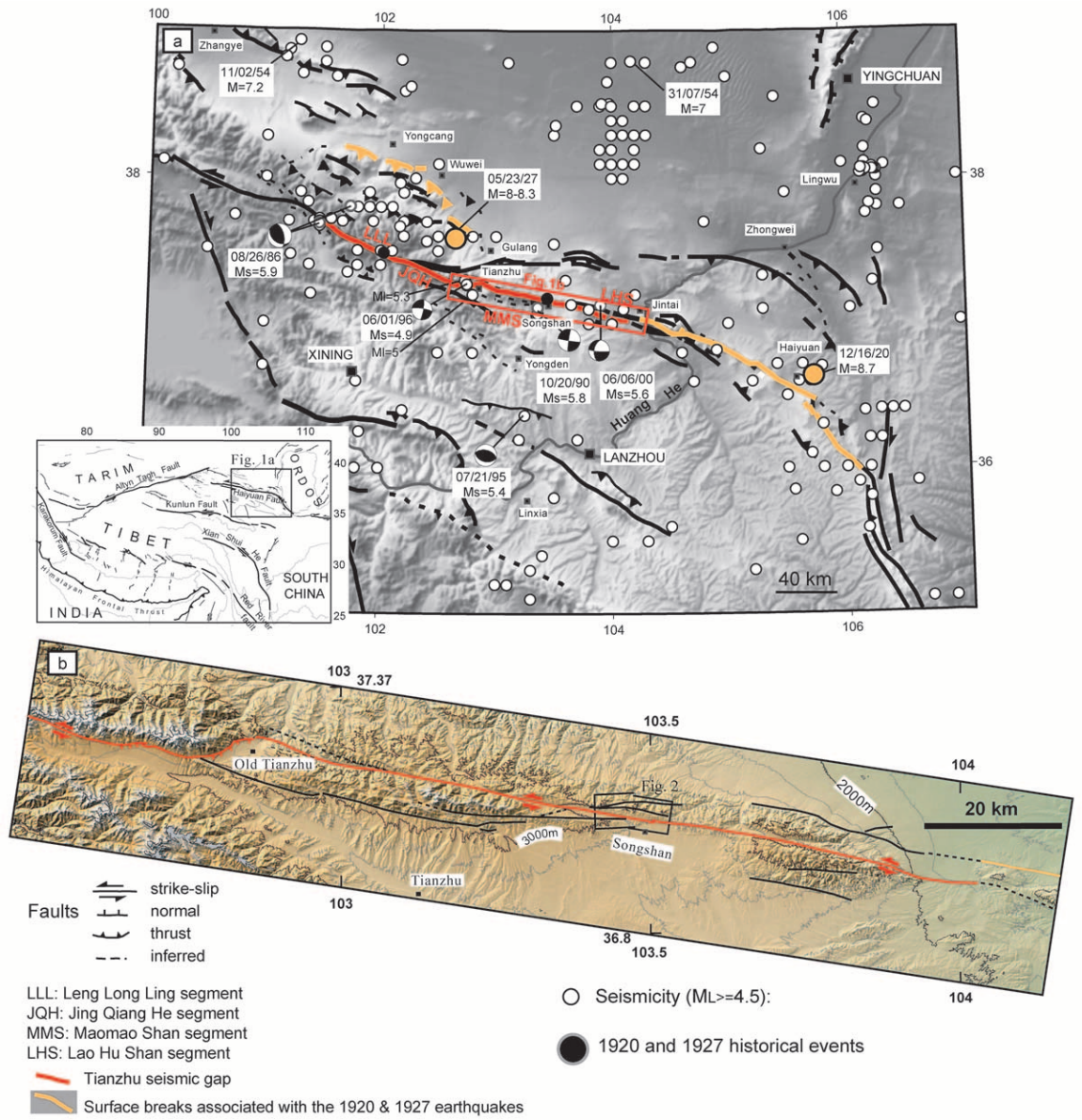

Figure 1. Tectonic setting of the Haiyuan fault. (a) Major active faults and historical earthquakes ($M_L \geq 4.5$) in the region adjacent to the Haiyuan fault. Surface ruptures associated with the 1920 and 1927 earthquakes are shown in orange. Tianzhu seismic gap is highlighted in red (after Lasserre *et al.*, 2001). (b) Surface traces of the Haiyuan fault system near Tianzhu and Songshan, superimposed on Shuttle Radar Topography Mission (SRTM) Digital Elevation Models (DEMs). Elevation contour interval is 250 m.

(Mériaux *et al.*, 2004, 2005) determined near 90° E along the Altyn Tagh fault differ by a factor of two. The GPS and Holocene rates of the Kunlun fault (11 ± 2 mm/yr), on the other hand, are now consistent within uncertainties (van der Woerd *et al.*, 2000, 2002; Wang *et al.*, 2001; Chen *et al.*, 2004; Zhang *et al.*, 2004). No definitive GPS results across the Haiyuan fault are available yet; GPS points from large-scale GPS studies in Tibet (e.g., Wang *et al.*, 2001; Zhang *et al.*, 2004) are too sparse to adequately constrain the present rate. Preliminary results from two campaign GPS profiles east and west of Songshan (Lasserre, 2000) seem to indicate a lower rate than the 8–16 mm/yr Holocene rate determined by Gaudemer *et al.* (1995) and Lasserre *et al.* (1999, 2002).

Discrepancies between GPS and geomorphic rates on active faults are not unique to Tibet. They are also found, for instance, on the Blackwater fault in southern California, the geodetic rate being four times higher than geologic rates (Dokka and Travis, 1990; Miller *et al.*, 2001; Peltzer *et al.*, 2001; Oskin and Iriondo, 2004). Understanding the relationship between GPS and geological rates is a fundamental issue. Possible reasons for such discrepancy could be incompleteness of the paleoseismologic/geologic record or

assumptions about rheologic properties of the crust and fault geometry used to model GPS data. However, the most probable reason for discrepancy may be the difference in the duration of the observational period. Present GPS measurements record motions for at most a couple of decades of elastic strain accumulation, a period much shorter than the seismic cycle, whereas Quaternary geologic rates derived from dated geomorphic offset markers yield values averaged over periods of thousands of years (10–100 ka). How short-term elastic deformation is converted with time into long-term permanent unrecoverable strain is not fully understood. Short-term fault-loading rates may vary with time because of interaction between conjugate or adjacent faults (Peltzer *et al.*, 2001; Hubert-Ferrari *et al.*, 2003), prior fault-rupture history and postseismic relaxation (Stein *et al.*, 1997; Dixon *et al.*, 2000, 2003), or the rheology of the crust and mantle below the seismogenic zone (e.g., Segall, 2002; Perfettini and Avouac, 2004). Without quantitative knowledge of multiple deformation cycles, it remains difficult to understand the present-day motions and recent tectonic evolutions of most fault systems.

Because paleoseismology addresses the issue of how frequently large earthquakes occur on a fault, it provides information on repeated fault motion during several earthquake cycles, in time windows of hundreds to thousand of years. Thus, it has adequate temporal resolution to fill the gap between current GPS measurements and geomorphic studies of active faults. For this reason, we have started a multiyear project to systematically investigate the paleoseismic behavior of active faults in Tibet. As a step toward this goal, this article presents our initial effort on the Haiyuan fault.

Seismotectonic Setting

Together with the Altyn Tagh, Kunlun, and Xianshuihe faults, the ~1000-km-long, active left-lateral Haiyuan fault accommodates part of the eastward component of movement of Tibet relative to the Gobi-Ala Shan platform to the north (e.g., Peltzer *et al.*, 1988). It branches off the Altyn Tagh fault in the Qilian Shan mountain range, and continues eastward, striking about N110°. It then veers to a N140° strike east of the Yellow River, and to a ~north–south strike along the edges of the Liupan Shan, and resumes a N100° strike again before merging with the northern boundary of the Qinling Shan. By dating offset lateral moraines at a site near 101.85° E, Lasserre *et al.* (2002) determined that the Late Pleistocene average slip rate on the westernmost Haiyuan fault is 19 ± 5 mm/yr. This rate decreases to 12 ± 4 mm/yr, constrained by dated offset alluvial terraces, east of the junction between the Haiyuan and Gulang faults, with the latter probably accommodating about 4 mm/yr (Gaudemer *et al.*, 1995; Lasserre *et al.*, 1999). In less well-circulated Chinese literature, however, the left-slip rate between 102° E and 104° E is estimated to be less than 5 mm/yr using offset river terraces (He *et al.*, 1994, 1996; Yuan *et al.*, 1998). This estimate, however, is not constrained by the dating of individual offset terraces, but by using inferred ages based on regional correlation of terraces and climatic events. East of the Yellow river, Zhang *et al.* (1988) derived a rate of 8 ± 2 mm/yr, a value intermediate between those mentioned previously. Though, strictly speaking, only lower bounds of the rate were constrained at various sites, Zhang *et al.* (1988) concluded that 8 ± 2 mm/yr likely represented the possible range of the slip rate.

No consensus exists on the total offset and inception age of the Haiyuan fault. The Yellow River has an apparent left-lateral deflection of ~90 km where it crosses the fault (Fig. 1a). This has been inferred to represent the total left-lateral displacement on the fault since ~8 Ma (Gaudemer *et al.*, 1989, 1995). Based on geologic mapping along a 60-km stretch of the fault, Burchfiel *et al.* (1991) derived a total displacement of only 10.5–15.5 km and inferred that the left-lateral slip began near the end of Pliocene time (1.8 ± 0.3 Ma). Ding *et al.* (2004) used the development of pull-apart basins along the fault to argue for a total offset of ~60 km since 10 Ma.

During the past century the Haiyuan fault system (*sensu lato*) has produced two great earthquakes: the *M* 8.6 Haiyuan earthquake in 1920, along the eastern Haiyuan fault, and the *M* 8–8.3 Gulang earthquake in 1927, likely on a thrust-fault system north of the western Haiyuan fault (Fig. 1). The earthquake of 16 December 1920 produced a 237-km-long rupture, now well mapped, with a maximum left-lateral slip of 10–11 m, and claimed over 220,000 lives (Deng *et al.*, 1986; Zhang *et al.*, 1987; Institute of Geology, China Earthquake Administration and Ninxia Bureau of China Earthquake Administration, 1990). The rupture, spanning several fault segments, extended along the eastern part of the fault east of the Yellow River. The western end of the rupture was located just south of Jingtai, west of the bend of the Yellow River (Fig. 1). The mainshock was followed a week later, on 25 December 1920, by an aftershock with magnitude ~7 located less than 50 km east of the epicenter of the mainshock (Institute of Geology, China Earthquake Administration and Ninxia Bureau of China Earthquake Administration, 1990). The slip curve of this earthquake is bell shaped, with the maximum slip in the center, decreasing toward either end (Institute of Geology, China Earthquake Administration and Ninxia Bureau of China Earthquake Administration, 1990). Seven years later, the earthquake of 23 May 1927 occurred north of the Haiyuan fault, between 102° and 103°. It activated a south-dipping thrust, inferred to branch off from the Haiyuan fault at depth (Fig. 1a) (Gaudemer *et al.*, 1995; Lasserre *et al.*, 2001).

Several paleoseismic studies have been undertaken along the 1920 rupture (Zhang *et al.*, 1988; Institute of Geology, China Earthquake Administration and Ninxia Bureau of China Earthquake Administration, 1990; Ran *et al.*, 1997; Xiang *et al.*, 1998; Min *et al.*, 2000) to better assess the long-term hazard related to the occurrence of such a destructive

earthquake. The earthquake history of the Haiyuan fault west of Jingtai has raised much less interest.

The 260-km-long stretch of the Haiyuan fault (marked red in Fig. 1b) is composed of four segments. Despite clear evidence of Holocene activity in the field, this section of the fault bears no historical record of a large earthquake in the past several centuries. It has therefore been considered a major seismic gap (the "Tianzhu gap") with rather high potential seismic hazard (Gaudemer *et al.*, 1995). The 1920–1927 sequence of great earthquakes has lead to speculation that the Tianzhu gap would be the next section to break, in view of growing evidence for temporal clustering of earthquakes, in domino-type occurrence on single faults or fault systems (e.g., Sykes *et al.*, 1981; Barka *et al.*, 1992, Stein *et al.*, 1997). Moreover, the pattern of modern seismicity along this part of the fault is suggestive of concentrated loading along this gap (Lasserre *et al.*, 2001), and thus heightened seismic hazard. Figure 1a shows that after 1985, *M* 5–6 earthquakes cluster near the two ends of the gap region, and in the middle (Tianzhu pull-apart basin, the largest geometrical complexity on this stretch of the fault). This pattern is in sharp contrast with the diffuse and random modern seismicity along the section that broke in 1920, where crustal stress was likely relaxed for many decades after the great earthquake.

Site Description

To better assess the seismic hazard along the Tianzhu gap, and to investigate the frequency of large-earthquake occurrence on this fault, we have conducted paleoseismic investigations at a site near 103.5° E, in a small pull-apart basin, a few kilometers north of the village of Songshan (Figs. 2 and 3). Near the Songshan site, the fault cuts through a landscape of subdued topography, mantled by loess (Fig. 3). Because of the spectacular fault trace, clear geomorphic records of cumulative offsets and the easy access, the area had been targeted by Gaudemer *et al.* (1995) and Lasserre *et al.* (1999) to determine the Holocene slip rate of the fault. A detailed description of the geologic and geomorphic setting of the site is given in Gaudemer *et al.* (1995).

The excavation site selected is located at the eastern end of a left-stepping extensional jog, along the main fault trace. Figure 3 shows a photo looking south toward the basin and trench locations. The two fault strands that bound the basin are clear in the field. The northern strand, in particular, truncates alluvial fans, forming a south-facing scarp of up to 1 m locally. At the base of the scarp, a spring currently supplies water to a 3-m-deep river channel at the southeast corner of the basin. Toward the west, however, the northern strand disappears, possibly because it is covered by fast-depositing fans, or due to diminished fault slip, or both. The southern fault strand, associated with an upslope-facing scarp up to 0.5 m in places (Figs. 3 and 4), is geomorphically clearer than the northern strand and can be continuously traced toward the west.

Deposition in the basin originates from several small catchments on the northern slope. These small drainages build fans with toes extending into the basin. Although the basin is currently drained by a stream, it could have once been closed, judging from the smooth and flat basin floor and vegetation characteristics.

Stratigraphy

We opened two trenches across the two bounding fault strands. Trench 1, ~25 m long, 4 m wide, and 3 m deep, was excavated across the southern strand. Trench 2, dug across the northern strand, provided only limited exposure due to the shallower depth of the water table, ~2.2 m below ground surface. Each wall was systematically cleaned, gridded in squares of 1 m by 1 m using a total station, and photographed. The detailed field mapping of trench exposures was performed on printouts of photos of individual grid cells.

Figures 5a and 5b show an overview of the stratigraphy exposed in trenches 1 and 2, respectively. The sediments in trench 1 are mostly composed of fine-grained sand, silt, and clay indicating a low-energy depositional facies. Pebbles and coarser clasts are uncommon, likely because of the distal position of the trench relative to feeding catchments. Based on the similarity of facies, texture, and color, we divide the stratigraphy into three sections: lower, middle, and upper sections (Fig. 5).

The upper section, about 1 m thick, mainly consists of massive homogeneous sandy silt, interpreted as loess or reworked loess (Table 1). A couple of organic-rich soil horizons have developed. Bioturbation is extensive in this section, as indicated by large burrows and deep-penetrating roots of dry-land plants.

The middle section is mainly composed of two types of layers: light yellowish brown sandy deposits and thin dark-brown to black peatlike layers (Table 1). The preservation of fine layers (5–10 cm) and the presence of dark layers suggest that, at the time the middle section was emplaced, the water table was close to the surface, preventing strong bioturbation from burrowing and growth of dry-ground vegetation.

In contrast with the middle section, the lower section is darker; alternation of dark- and light-color layers is less common. It consists of clayrich, fine deposits, and is thus more coherent. The deposits may represent continuous marsh deposits, as exposed by trenching in similar environments, which often show massive deposits of dark-gray clay with few stratigraphic markers (Rockwell *et al.*, 1986).

Figure 5c is a composite stratigraphic section illustrating the representative thickness of individual units and stratigraphic locations of charcoal samples discussed later in the text. We did not illustrate the grain size and texture of individual layers because most of the deposits are homogenous sand and silt. Color contrast is the most significant difference. Most units, from 1 through 14, are laterally continuous and can be mapped across the fault zone with confidence.

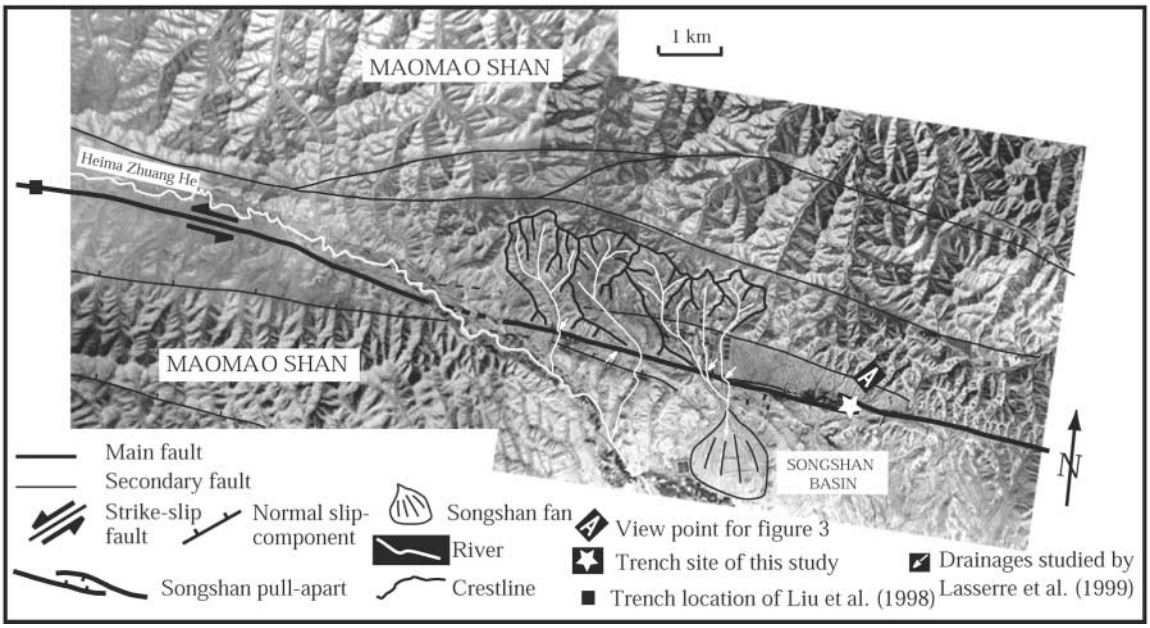

Figure 2. Map of the Haiyuan fault near Songshan, superimposed on aerial photos (modified from Lasserre *et al.*, 1999). Thick black line in the middle indicates the trace of the Haiyuan fault. Paleoseismic site described in this study (shown as a star) is located in the pull-apart basin north of Songshan village. Small drainages north of Songshan are highlighted in white, as is the Heimazhuang river, the major perennial river in this area. The locations of Lasserre *et al.*'s (1999) slip-rate determinations are indicated by white arrows. The location of a previous paleoseismic investigation site by Liu *et al.* (1998) is shown by a square, just outside the map area on the left.

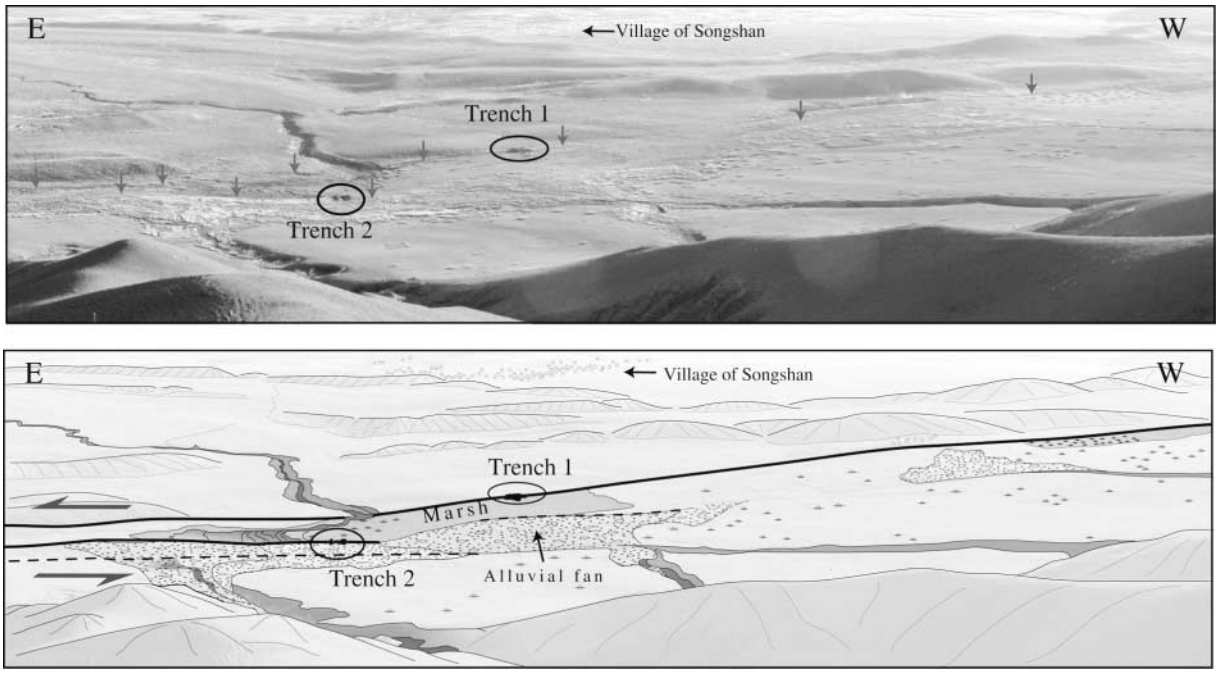

Figure 3. Mosaic of south-looking photos of the Haiyuan fault north of Songshan village and corresponding geomorphic interpretations. Locations of fault traces are indicated by red arrows. The southern strand coincides with a vegetation transition line. Trench 1 is located across the southern fault branch, and trench 2 is across the northern fault branch.

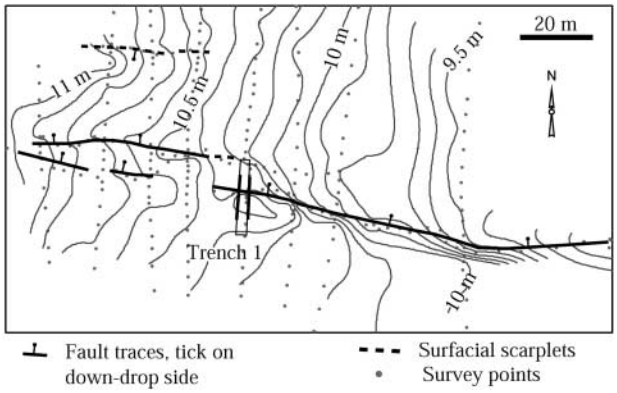

Figure 4. Topographic map derived from total station survey points (dots) near trench 1. The location of trench 1 is indicated by the rectangle in the middle. Logged portions of exposures are indicated by bold lines. In the vicinity of trench 1, the fault forms a north-facing scarp, about 0.5 m high in the east and decreasing westward. At the location of trench 1, the scarp is only about 10–15 cm high. Contour interval is 10 cm.

Correlation of units from trench 1 to trench 2 is primarily based on the identification of the three main sedimentary packages (Fig. 5c and Table 1). The transition between the top and the middle section is sharp, denoting a dramatic change from wet to dry climatic or hydrologic conditions at this location. In trench 2, the stratigraphic transition from the upper to the middle section is as sharp as in trench 1, confirming that the change from wet to dry was recorded basinwide. The one-to-one correlation of individual units is more difficult. Only the correlation of unit 2 is constrained by charcoal samples of similar age. Other unit correlations are based on qualitative observations. We reason that major gravel layers in trench 2, representing flooding periods, must be correlated with the main lighter-colored layers in trench 1. Thus, equivalents of units 5, 7, and 15 are determined. Such correlation is probable, because alternation of black-and-white thin layers between units 7 and 15 would be in the same stratigraphic position in both trenches.

Evidence of Faulting Events

In this section, we present and discuss stratigraphic evidence for six paleoearthquakes at the site. We name these events SS1 through SS6 from the youngest to the oldest.

Among various indicators for recognizing paleoearthquakes in unconsolidated sediments in a strike-slip fault setting, the best and clearest evidence of fault rupturing of the ground surface includes scarp formation, scarp-derived colluvium, in-filled and void fissures, and sand blows (e.g., Sieh, 1978; Weldon *et al.*, 1996; Fumal *et al.*, 2002). Upward fault terminations are most effective in identifying the most recent faulting event, but may not be as reliable for older events because subsequent ruptures sometimes follow the same plane and may overprint the evidence of previous events (Weldon *et al.*, 1996).

Most Recent Event (SS1)

Event SS1 appears to be a minor cracking event that probably ruptured the present ground surface (Figs. 6 and 7).

Multiple cracks on both walls of trench 1 can be traced confidently up to about 20 cm below the ground surface. The actual level of termination of these cracks, however, remains ambiguous because of loose loam near the surface. These cracks are not roots. They are not as straight and continuous as plant roots, but instead resemble *en echelon* cracks in a vertical plane. Voids at corners (Fig. 7), where the cracks change orientation, and visible clean shearing planes devoid of roots also argue for a tectonic origin. These cracks, however, show no offset in the underlying sedimentary layers. This suggests that the event corresponds to a small-magnitude earthquake, or was near the rupture termination of a somewhat larger one.

Analysis of the recent, local seismicity supports a tectonic origin for the cracks. Probably they are associated with the 20 October 1990 M_w 5.8 earthquake, whose reported epicenter was located at ~37.1° N and 103.5° E (Gansu Bureau of China Earthquake Administration, 1990; Committee for Chinese Earthquake Bulletin, 1990). This earthquake was the biggest event in Gansu province since the 1954 Shandan earthquake (M_s ~7.3). It caused severe damage (intensity VIII) in villages along a 27-km-long stretch of the Haiyuan fault, from the Heima Zhuang river (Fig. 2) eastward. The long axis of the intensity distribution had the same orientation as that of the Haiyuan fault, as did one plane of the focal mechanism (Gansu Bureau of China Earthquake Administration, 1990). Surface *en echelon* tensional cracks with up to 10 cm of opening were reported in the highest-damage area (intensity VIII), 7 km to the southeast of our paleoseismic site (Fig. 8). No exhaustive investigation was carried out to trace the extent of cracks shortly after the earthquake. Although ground fissures were observed in many places, only those in the maximum-intensity region (intensity VIII) were believed to be of tectonic origin. In the village of Songshan, which is quite close to the epicenter, there were many accounts of building damage; pillars or columns moved counterclockwise relative to the ground, most likely indicating near-field ground motion rather than far-field oscillation. The walls of the small ancient fortified city (Songshan), erected sometime during the Ming Dynasty (1368–1644 A.D.), which were mostly standing intact before this earthquake, partially collapsed (Gansu Bureau of China Earthquake Administration, 1990; Gaudemer *et al.*, 1995).

Together, the consistent reports suggest that the October 1990 earthquake may have been large enough to produce ground rupture extending several kilometers away from the epicenter. As our excavation site is located closer to the instrumental epicenter than the reported tectonic cracks, it

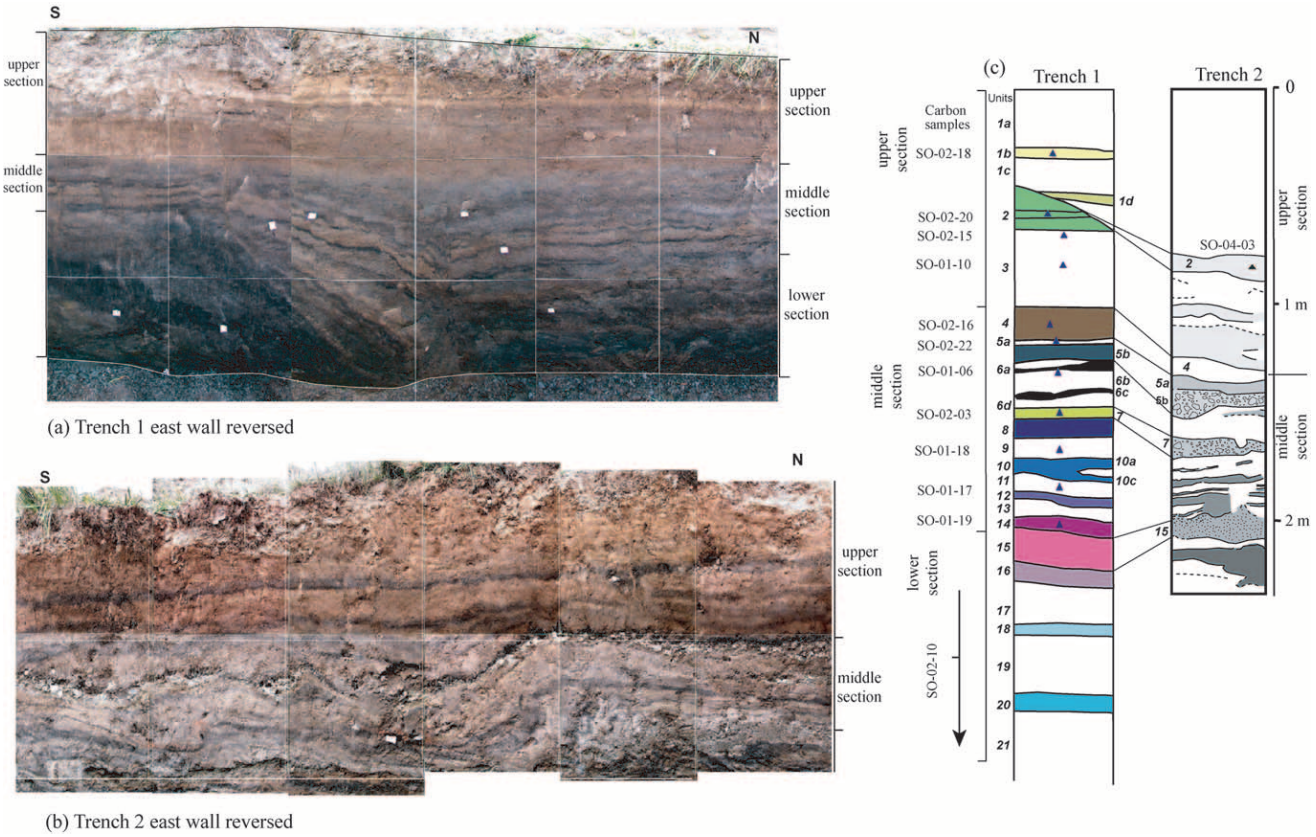

Figure 5. Photo mosaic of central section of the eastern walls of trench 1 (a) and trench 2 (b) showing the general characteristics of the stratigraphy and the tilting and warping of strata due to deformation. Stratigraphy is divided into upper, middle, and lower sections. Photos were reversed as if looking toward the west. (c) Generalized stratigraphic column of sedimentary deposits in trenches 1 and 2, and proposed correlation between the two trenches. We label units in trench 1 from 1 to 21, from top to bottom. Color coding corresponds to Figures 6 and 10. Stratigraphic position of radiocarbon samples are shown by triangles.

Table 1
Unit Descriptions from Trench 1 and 2 Exposures

	Unit No.	Trench 1	Trench 2
Upper section	1	Bioturbated silty loess and reworked loess. Subunit 1b is a distinctive thin layer, better sorted and lighter in color than units above and below. Subunit 1d is a darker organic-rich layer.	Massive bioturbated light yellowish brown sand and silt.
	2	Gray organic-rich sand and silt, containing a discontinuous carbonate layer.	Dark-gray organic-rich sand and silt.
	3	Massive yellow to brownish yellow sand and silt.	Massive yellow to brownish yellow sand and silt, with multiple dark organic-rich soil horizons.
Middle section	4	Wedge-shaped deposit of gray clayey sand and silt	
	5	5a: A thin layer of silt, on the up-thrown side of the fault. 5b: Pale-yellow silty sand, on the down-thrown side of the fault.	Clast-supported gravel layer of angular to subangular pebbles.
	6	Brownish sandy silt, locally containing dark organic-rich layers.	
	7	Pale-yellow silty sand.	Clast-supported pebbly to granular gravel in coarse sand matrix.
	8–14	Alternating dark peatlike layers (units 8, 10, 12, and 14) and light yellowish brown coarser-grained silty sand (units 9, 11, and 13).	Alternating thin, dark organic-rich layers and white to light-gray clayey silt.
Lower section	15	Gray sand and silt.	Relatively well-sorted coarse and medium sand.
	16–21	Alternating brown clayey sand and silt (units 16–20) and dark gray finer-grained clay (units 17, 19, and 21).	

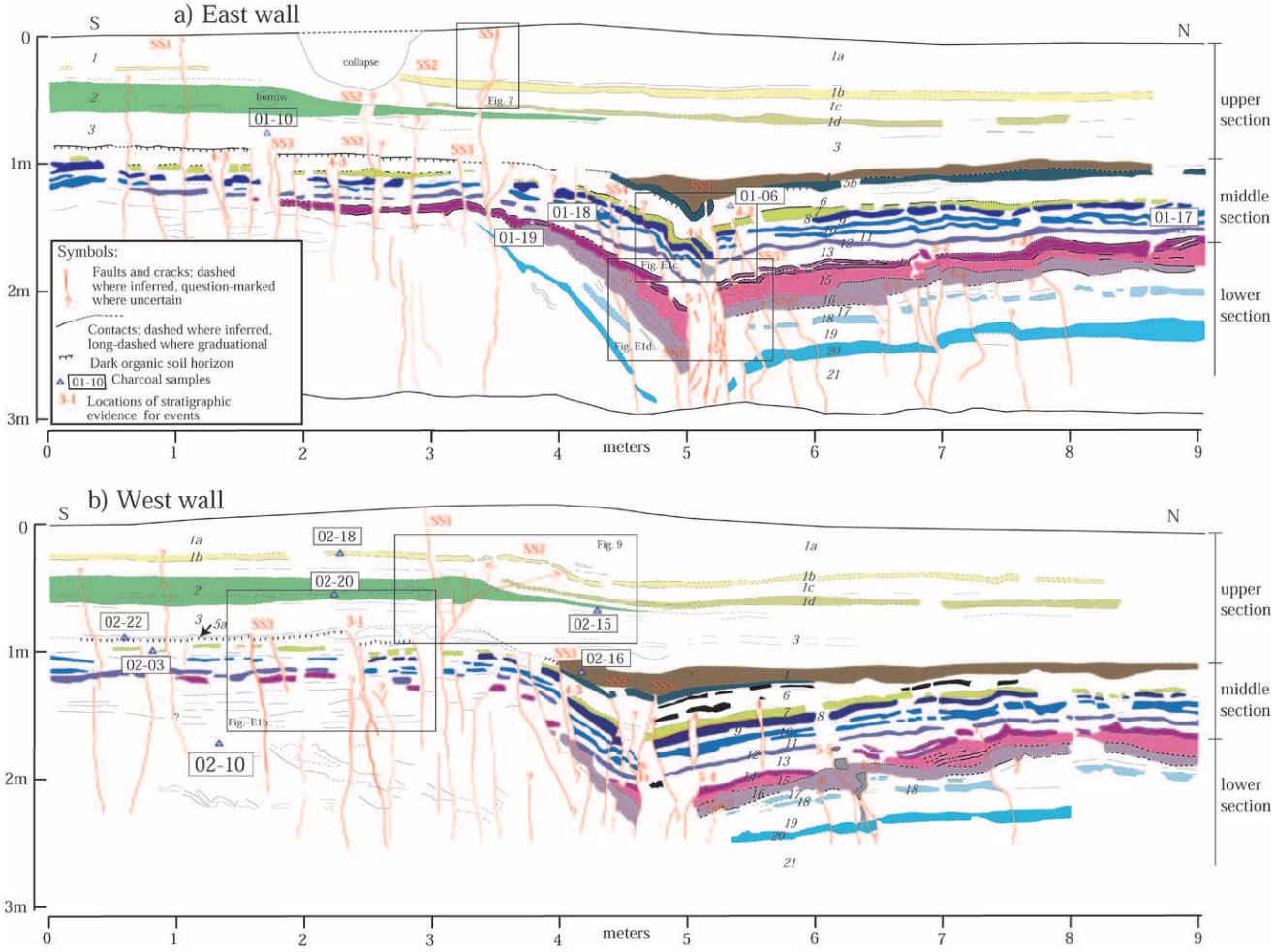

Figure 6. Logs of portions of the east (a) and west (b) walls of trench 1. Sedimentary units are indicated by different colors and are labeled numerically. Ruptures associated with six events are identified and named SS1, SS2, SS3, SS4, SS5, and SS6, from the youngest to oldest. See text for description of evidence of individual events.

seems likely that the cracks observed in the trench walls are indeed tectonic cracks due to the 1990 event.

Penultimate Event (SS2)

Evidence for Event SS2 in Trench 1. The next youngest deformation event we identify prior to event SS1 occurred when unit 1b was at or near the surface. The clearest evidence for event SS2 in trench 1 is the convex-upward, bulging out of unit 1b in the fault zone, between meters 3 and 4 in the western wall (Figs. 6b and 9). Unit 1b is a distinctive 5-cm-thick layer of silty fine sand that is continuously traceable on both walls of trench 1. It is lighter in color and better sorted than the sediment layers below and above. It is likely an aeolian deposit, or less likely a flood deposit. The convex-upward shape of unit 1b near meter 4 is probably an indication of folding. Below unit 1b, faults exhibit a flowerlike structure offsetting both the upper and lower surfaces of unit 2 and possibly unit 1d as well. The offset is not large, no more than a couple of centimeters in a vertical plane. The underlying layers (i.e., unit 5 and those below) also do not display large vertical separation. This pattern is typical of *en echelon* ground ruptures forming small pressure ridges at the surface with only strike-slip motion at depth (e.g., Yeats *et al.*, 1997; Barka *et al.*, 2002).

Unfortunately, we cannot be sure that the bulging of unit 1b is an indication of coseismic deformation because of the bulging is quite small and subtle. Alternatively, unit 1b may have been deposited after event SS2 and mantled the scarp. In the eastern wall exposure, a few cracks seem to extend through layer 1b, which would support the former interpretation. But this is not conclusive because plants can take advantage of pre-existing cracks. The key area in the east wall was accidentally destroyed during excavation (Fig. 6a).

Evidence for SS2 in Trench 2. Stronger stratigraphic evidence for SS2 is found in trench 2 (Fig. 10 and Ⓔ Fig. E1a in the online edition of BSSA). Fissures cut through unit 2,

Figure 7. Enlarged photo of eastern wall of trench 1 showing that the crack associated with the youngest event SS1 (outlined by black arrows) appears to extend to the ground surface. We believe this event is the 1990 M_w 5.8 earthquake. See location in Figure 6.

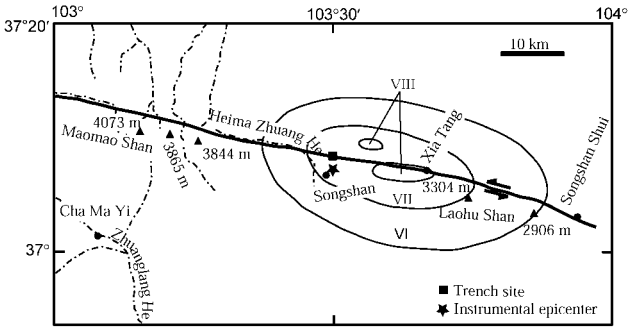

Figure 8. Map of intensity associated with the 1990 M_w 5.8 earthquake. Adapted from Gansu Bureau of China Earthquake Administration (1990).

down-drop blocks from unit 2, and fissure fills are clearly associated with this event. The organic-rich layer, unit 2, is disrupted with a few centimeters of vertical separation. Sediments from this layer form part of the colluvium that fell into the fault zone. A cobble, about 6–7 cm in diameter, located in the fault zone, does not correspond to any fine-grain-sized unit characteristic of the upper section in trench 2, and has probably been dragged into the fault zone. The fissure is filled with sediments lighter in color, most likely from layers above unit 2. The fissure fill and colluvium suggest that the event horizon is slightly above unit 2. There is also indication of strike-slip motion along the fault in trench 2. The thickness of unit 2 changes across the fault zone, being thicker on the northern side than on the southern side (Fig. 10).

Event SS3

Evidence for Event SS3 in Trench 1. Unlike events SS1 and SS2, event SS3 is associated with a wide zone of deformation, 4 to 5 m in total, which suggests that event SS3 probably had larger offset than SS1 and SS2. Figure 6 shows that event SS3 involves both shearing on the main fault zone and offsets on multiple secondary faults between meters 1 and 4. Some of the best evidence for event SS3 is preserved along the southern half of trench 1, outside the main fault zone (denoted "3-1" on the west wall, Fig. 6b Ⓔ and Fig. E1b in the online edition of BSSA). Unit 5a buries a dark organic soil horizon on top of unit 6. The soil horizon is easily traced in both the east and west walls. Unit 5a, together with the soil horizon beneath it, is sharply offset by three secondary fissures, with about 7 cm of vertical separation. Material from unit 3, a massive loess layer, usually fills these fissures, delineating open cracks up to 1 m deep. At approximately meter 2.5 on the west wall (Fig. 6b and Ⓔ Fig. E1b in the online edition of BSSA), a secondary fault limits chunky deposits that appear to be broken pieces of the underlying layers. These blocks are probably coseismic colluvium, transported here from locations out of the section plane. They are separated by infilling of unit 3 sediments.

Combining the deformation on the main fault and secondary faults, the overall effect of event SS3 is a down-drop of the block located north of the main fault zone, together with northward tilting and dragging of unit 5b and of all the units below, most prominently south of the main fault. The event horizon should be slightly above unit 5a because units 5a and 5b are disrupted. Unit 4, a wedge-shaped deposit of light-gray clayey sand and silt north of the main fault zone, which thickens above it, is likely the postevent in-fill of the depression produced by event SS3.

Evidence for Event SS3 in Trench 2. Evidence for event SS3 in trench 2 is different from the cracks exposed in trench 1. The stratigraphy shows strong ductile-style folding (Fig. 10). This style of deformation would be consistent with strong ground shaking in water-saturated deposits during an earthquake. Unit 5, a gravel layer, is the top most deformed layer. Layers located above are much less contorted and clearly drape unit 5. Hence, the event horizon associated with event SS3 is probably at, or slightly above, unit 5. It would be ambiguous to locate the position of ground surface if units 1 through 5 were subaqueous soft sediments when the earthquake occurred (e.g., Weldon *et al.*, 1996). This is not the case at the Songshan site, because units 1 through 4 consist of subaerial deposits. They are loess and reworked loess with multiple soil horizons developed subaerially.

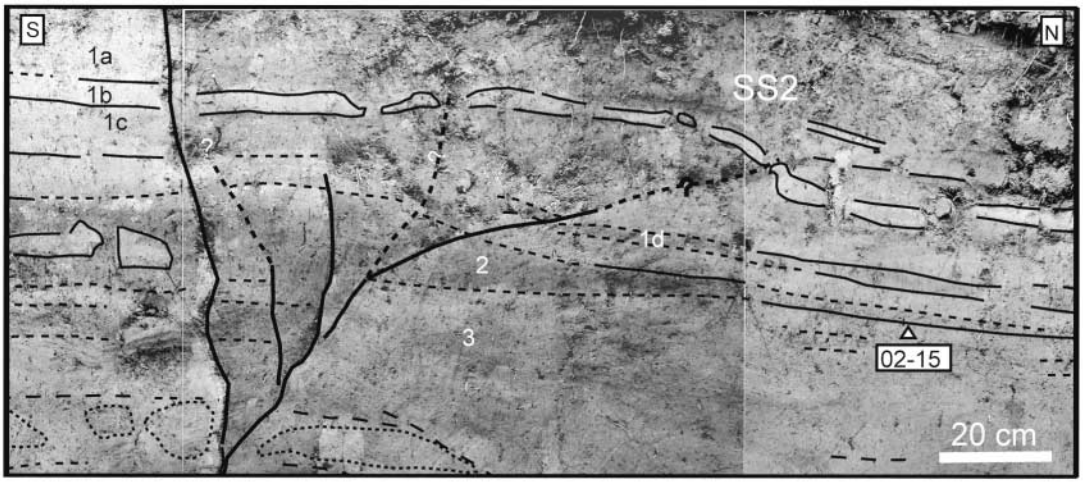

Figure 9. Photo mosaic and interpretations of a portion of the western wall of trench 1 showing the evidence for event SS2. See location in Figure 7.

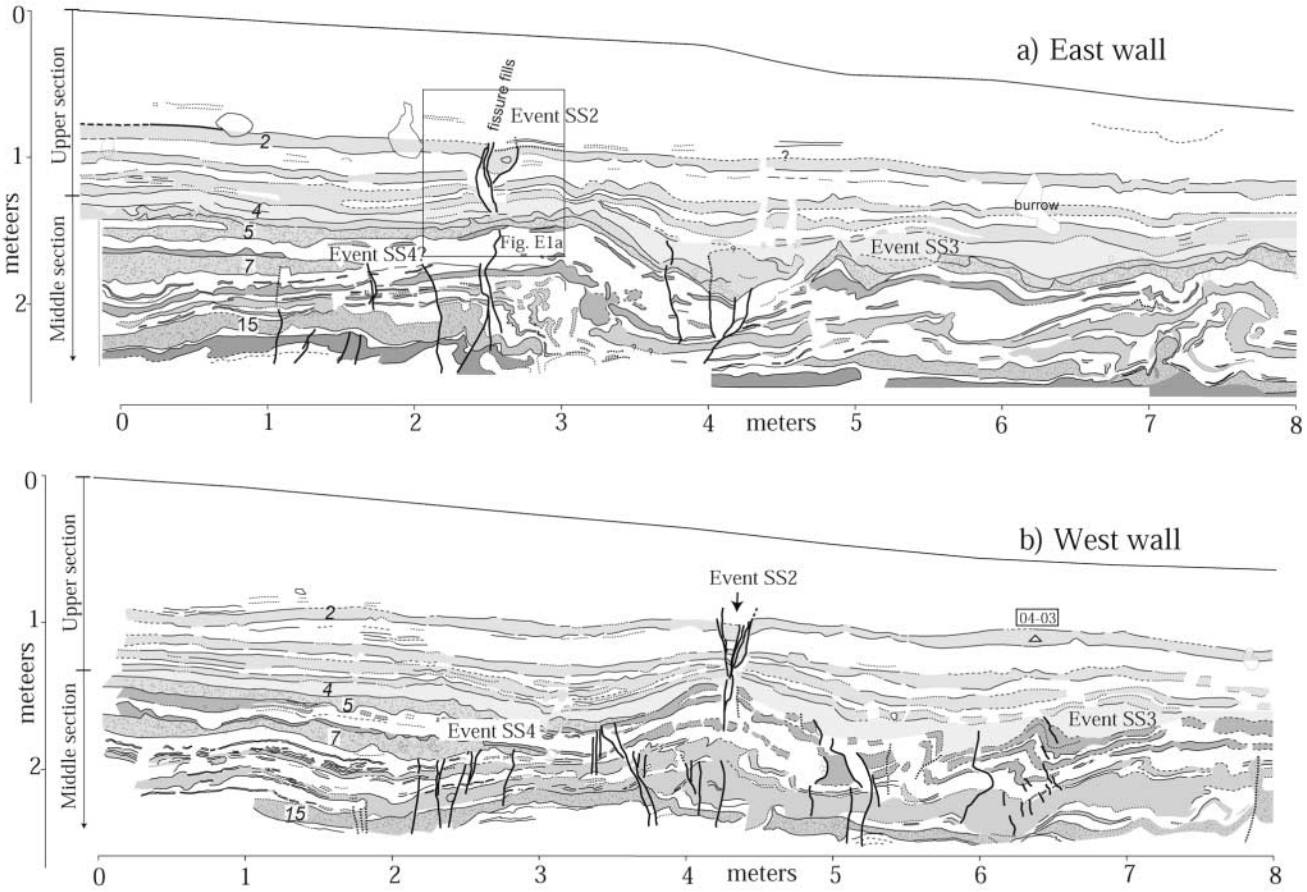

Figure 10. Logs of the east (a) and west (b) walls of trench 2 depicting the stratigraphy and deformation associated with events SS2, SS3, and SS4. See legend in Figure 6 for explanation of symbols.

Coarser grain size, the lack of clay in the sediments, and deeply penetrating plant roots corroborate this subaerial interpretation.

Event SS4

Fault breaks associated with event SS4 disrupt the upper surface of unit 7 over a width of several meters and terminate within unit 6 of trench 1 (Fig. 6). Multiple strands terminate at this stratigraphic position. The strongest evidence for the event is within the fault zone on the east wall, at meter 5, where a major shear plane separates the coherent strata of units 7 to 12 to the left from a mélange of sheared material to the right (designated "4-1" on Fig. 6a and Ⓔ Fig. E1c in the online edition). The fault is capped by a small duplex of units 7 and 8, thrust on top of one another, which suggests that this layer was at or very near the ground surface when rupture occurred. Additional evidence includes a fault strand north of the main fault (designated "4-2" in Fig. 6a and Ⓔ Fig. E1c in the online edition) offsetting unit 7 by a few centimeters; and at least two open cracks south of the main fault (designated "4-3" in Fig. 6a) terminating in the same stratigraphic position.

Although events SS3 and SS4 are only separated by unit 5 and 6 deposits with only about 40 cm in total thickness, multiple lines of evidence suggest that they are distinctly separate events. First, at locations 4-1 and 4-2, unit 7 and underlying units are warped more and thus deformed more than the overlying unit 5. This difference between unit 5 and underlying unit 7 requires an event horizon after the deposition of unit 7. Second, at location 4-3, the stratigraphic contacts show clearly that the open cracks of event SS4 terminate below the sharp soil horizon developed in the top of unit 6, whereas fault strands associated with event SS3 offset this horizon. Inside the cracks, fissure fills of event SS4 consist of material of unit 6, darker than those in the cracks of event SS3. Third, the change in thickness of unit 6 across the fault on the west wall is consistent with a pre-existing scarp, presumably due to event SS4 (Fig. 6b). Also, unit 6 is thickest near the main fault zone. It thins out northward away from the main fault zone on the down-thrown north side. Southward, it stops abruptly against the southern-bounding fault and cannot be traced farther away from the fault on the up-thrown side. Thus the wedge-shaped thickness of unit 6 suggests it filled a sag created by a north-facing fault scarp. The subsequently deposited unit 5 has similar variation in thickness, but it is less conspicuous because of the more subdued scarp relief after filling by unit 6 on the north side.

Like event SS3, event SS4 in trench 2 manifests itself by sediment warping and folding in both walls. The event horizon of SS4 is less clear in trench 2 because of the superposition of deformation due to event SS3. Event SS4 probably occurred after unit 7 was deposited, because the layers below unit 7 are more deformed than units above.

Event SS5

Evidence for event SS5 is manifested in several places in trench 1. Fault traces from event SS5 break unit 14 (Fig. 6). On the east wall, a fault separates unit 14 and underlying units on the south side from the heterogeneous shear-zone fabric on the north side ("5-1" on Fig. 6a and Ⓔ Fig. E1d in the online edition). The small fissures cracking unit 12 and higher do not seem to connect to the main crack-breaking unit 14 at location 5-1. Hence the fault ending at 5-1 seems to be capped by unit 12. Outside the main fault zone, a few minor faults, which terminate above the upper surface of unit 14 ("5-2" and "5-3"), provide additional evidence for event SS5 on the eastern wall. Evidence for event SS5 is also visible on the west wall, both within the main fault zone ("5-4") and beyond ("5-5"). The event horizon associated with event SS5 is probably at or above unit 14.

Event SS6

Evidence for event SS6 is best preserved at the northern end of trench 1. On the east wall, several minor faults break unit 16 ("6-1" and "6-2" on Fig. 6a), producing a south-facing scarp and the greater thickness of unit 15 between this scarp and the main fault zone. On the western wall, unit 16 also displays evidence of event SS6. A mound delineated by the thickness variation of unit 16 ("6-3" on Fig. 6b) probably represents a pressure ridge. Undisturbed unit 15 lies above unit 16, smoothing out the irregular topography after event SS6. The event horizon of SS6 is clearly unit 16.

Evidence for event SS6 at the main fault zone is less straightforward because of the large amount of shear due to later events. However, the angular unconformity between units 14 and 16 suggests that motion in the main fault zone caused these units to tilt during event SS6. As will be discussed later, reconstruction of the stratigraphy before and after event SS6 helps to elucidate this effect.

Radiocarbon Dating of Earthquakes

Numerous charcoal fragments were found in both trenches, yet most were small. Thirteen samples were sent for accelerometer mass spectrometer (AMS) dating at Universiteit Utrecht in the Netherlands and Laboratoire de Mesure du Carbone 14 (LMC 14) in France. Radiocarbon dates are summarized in Table 2 and Figure 11. The stratigraphic positions of the samples are shown in Figures 5, 6, and 10.

Figure 11a plots the ages of charcoal samples in trench 1 in stratigraphic order. Most samples yielded ages younger than 3000 years B.P. Two samples, SO-01-19 and SO-02-18 (Table 2 and Figs. 5 and 6), collected 0.3 m and 2.0 m below the surface yielded ages of 7080–7480 B.C. and 5840–6170 B.C., respectively. They are excessively older than the rest of samples and are most probably reworked charcoal fragments. Therefore we choose to not use them for age control. Two samples, SO-02-22 and SO-02-20, appear to be several

Table 2
Radiocarbon Samples

Sample	Laboratory No.	$\delta^{13}C$ (p. mil)*	Radiocarbon Age (Years B.P. ± σ)	Calendar Years† (cal B.P.) 1 σ	Calendar Years† (cal B.P.) 2 σ	Mass (mg)	Description	Unit Sampled
SO-01-06	12963‡	−32.6	1752 ± 44	230–350 A.D. 360–390 A.D.	130–160 A.D. 170–200 A.D. 210–410 A.D.	0.260	small piece of charcoal	6b, trench 1
SO-01-10	12964‡	−28.6	1180 ± 50	770–900 A.D. 920–940 A.D.	710–750 A.D. 760–990 A.D.	0.39	angular charcoal fragment, solid	3, trench 1
SO-01-17	12965‡	−26.3	2841 ± 38	1050–920 B.C.	1130–900 B.C.	0.380	charcoal	11, trench 1
SO-01-18	12966‡	−22.2	2674 ± 38	970–950 B.C. 930–890 B.C. 880–830 B.C.	1000–820 B.C.	2.23	charcoal	9, trench 1
SO-01-19	12967‡	−26	8258 ± 45	7450–7390 B.C. 7380–7290 B.C. 7270–7180 B.C.	7480–7130 B.C. 7100–7080 B.C.	1.56	charcoal	14, trench 1
SO-02-03	001603§	−24.3	1915 ± 45	20–140 A.D.	0–230 A.D.		charcoal	7, trench 1
SO-02-10	001602§	−27.4	3410 ± 45	1860–1840 B.C. 1770–1620 B.C.	1880–1790 B.C. 1780–1600 B.C. 1570–1530 B.C.		charcoal	below unit 16, trench 1
SO-02-15	12968*	−21.4	989 ± 35	990–1040 A.D. 1090–1120 A.D. 1140–1160 A.D.	980–1160 A.D.	1.140	small pieces of broken charcoal grain	3, trench 1
SO-02-16	12969‡	−23.3	1338 ± 49	650–720 A.D. 740–770 A.D.	600–780 A.D.	0.180	tiny piece of charcoal, treated only with acid	4, trench 1
SO-02-18	12970‡	−22.9	7150 ± 60	6160–6150 B.C. 6080–5980 B.C. 5950–5920 B.C.	6170–6130 B.C. 6110–5880 B.C. 5860–5840 B.C.	2.26	large piece of charcoal, solid	1b, trench 1
SO-02-20	12971‡	−22.1	393 ± 36	1440–1520 A.D. 1590–1620 A.D.	1430–1530 A.D. 1550–1640 A.D.	0.610	charcoal	2, trench 1
SO-02-22	12972‡	−23.2	1102 ± 28	895–925 A.D. 940–985 A.D.	890–1000 A.D.	0.690	charcoal	5, trench 1
SO-04-03	12973‡	−23.4	723 ± 38	1260–1300 A.D. 1370–1380 A.D.	1220–1310 A.D. 1350–1390 A.D.	2.30	charcoal	2, trench 2

*$\delta^{13}C$ (ppm), ratio of $^{13}C/^{12}C$ with respect to PDB reference.
†Calculated using OxCal program Version 3.5 (Ramsey, 2000), atmospheric data from Stuiver *et al.* (1998).
‡Universiteit Utrecht, Accelerator Mass Spectrometry facility, Utrecht, Netherlands. All samples were pretreated using AAA (acid-alkali/acid) method, except SO-02-16, which was treated only with acid.
§Laboratoire du Mesure du Carbone (LMC) 14, France.

hundred years younger than implied by stratigraphic ordering. In particular, sample SO-02-22 has an inverse stratigraphic age compared to two samples in overlying sediments. We have no reason to doubt the validity of this sample's age, a larger (0.6 mg) sample than the two preceding and retrieved from a well-defined sedimentary layer. Because of the detrital nature of our samples, the most plausible explanation is that older overlying samples may be reworked fragments. Discordant or stratigraphic inverse ages of detrital charcoal are common (e.g., Blong and Gillespie, 1978; Nelson, 1992; Grant and Sieh, 1993, 1994; Rubin and Sieh, 1997; Vaughan *et al.*, 1999; Rockwell *et al.*, 2000; Fumal *et al.*, 2002; Liu-Zeng *et al.*, 2006).

In Figure 11b, stratigraphic positions of event horizons are shown as filled rectangles. The horizontal dimensions of the rectangles indicate the age ranges of the events. They are loosely bracketed by the dates of samples from immediately older and younger units.

As previously discussed, we interpret event SS1 to be the 1990 M_w 5.8 earthquake. Event SS2 occurred after the deposition of sample SO-02-20, which has a calibrated age of 1430–1640 A.D. (2σ). We can further infer that event SS2

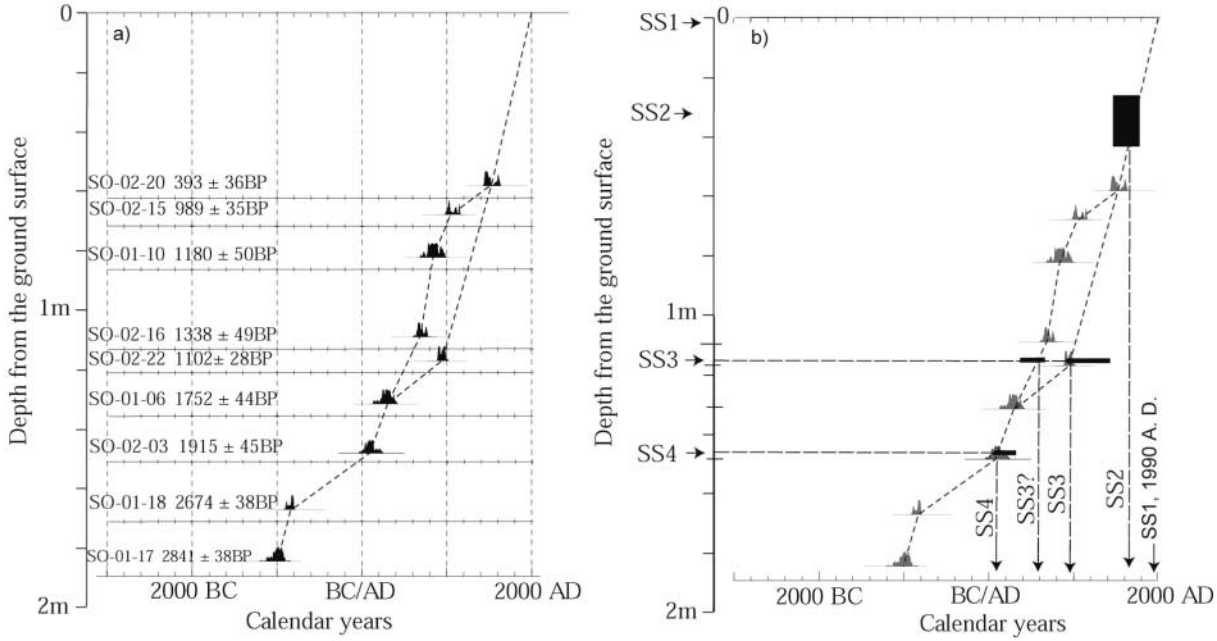

Figure 11. (a) Radiocarbon date ranges of samples from upper 2 m of sediments in trench 1, plotted in stratigraphic order. Two anomalously old samples, SO-01-19 and SO-02-18, probably due to reworking, are not included. Apparent stratigraphic age inversion of samples at about 1 m depth is probably due to reworked samples. (b) Constrained and inferred ages of four youngest events. Arrows and letters mark the stratigraphic levels of events. Horizontal bars indicate the bounds of event ages. The thickness of the box for event SS2 indicates uncertainty in the event horizon.

probably occurred before the Ming fortified city in Songshan was built, because the city walls were intact until the 1990 earthquake (Gansu Bureau of China Earthquake Administration, 1990; Gaudemer *et al.*, 1995). Because sample SO-02-20 has an age range almost the same as the duration of the Ming dynasty (1368–1644 A.D.), this age range probably includes the time of event SS2. Two interpretations of age for event SS3 are possible (Fig. 11b). Our preferred one is that the age of event SS3 is loosely bound by samples SO-02-22 and SO-02-20. It occurred some time after 890–1000 A.D. and before 1430–1640 A.D., but probably shortly after the deposition of unit 5a. Because unit 5a is thin, 2–4 cm, and the average sedimentation rate is rather fast (0.5–1 mm/yr as indicated by Fig. 11), event SS3 probably occurred in the eleventh or twelfth century. Another possibility for the age of event SS3, though not our preferred interpretation, is between the age bounds provided by samples SO-01-06 and SO-02-16. In keeping with this scenario, event SS3 would have occurred sometime after 130–410 A.D. and before 600–780 A.D. Using the OxCal program (Ramsey, 2000), we can infer a 2-σ range of 370–650 A.D. The timing of event SS4 is relatively well constrained by samples SO-02-03 and SO-01-06. In other words, it occurred sometime after 0–230 A.D., and before 130–410 A.D. Therefore, a conservative estimate of the age range for event SS4 is 0–410 A.D.

Sample SO-02-10, not shown in Figure 11, provides bounds on the ages of older events. It is located in an indistinctive unit on the up-thrown side of the fault, about 0.6 m below unit 14 (Fig. 6b). Its relation with units 15 though 21, however, is unclear because the stratigraphy on the up-thrown side is not well preserved enough to correlate individual layers with confidence. The 0.6-m depth of sample SO-02-10 below unit 14, if one assumes a similar sedimentation rate on both sides of the fault, suggests that the sample would date unit 19. This assumption is unlikely, however. The sedimentation rate is rather lower on the southern side, making the sample correlative to a deeper unit. In any case, sample SO-02-10 is located in sediments deformed by SS6 and therefore provides the lower-bounding age of our oldest event SS6. Its event horizon is unit 16, which has a 2-σ age range of 1530–1880 B.C. Thus, we conclude that all six events occurred during the past 3500–3900 years.

Discussion and Conclusions

Excavations at the Songshan pull-apart site expose stratigraphic evidence for six events during the past 3500–3900 years. Of these events, the four oldest are probably associated with large horizontal offsets, based on comparison of vertical separations and fault-zone widths. Event SS1 appears instead to be the minor, historical, 1990 M_w 5.8 earthquake. Thus, the four large events within 3500–3900 years would imply a recurrence interval of about 1000 years. Note that events with minor disturbance, such as event SS1

and perhaps SS2, could have occurred, but corresponding evidence cannot be retrieved because of overprinting of larger events. Thus, only the most recent of such events are recognizable. Therefore, we do not consider these smaller events in our estimate of earthquake recurrence. Charcoal samples within the uppermost 2 m of sediments indicate that, in addition to the 1990 earthquake and SS2, two large events occurred after 0–230 A.D. This is consistent with an average recurrence interval of about 1000 years.

Offsets of Events at the Site

Our trenching program at Songshan was not designed to determine the horizontal offsets of specific events. Nevertheless, based on vertical offsets, amounts of disruption and widths of deformation zones associated with each event, we may infer qualitatively the relative sizes of events.

Four of the events, SS3, SS4, SS5, and SS6, appear to be large surface-rupture earthquakes. The vertical offsets are best determined for these events through restoration of strata before and after each event (Fig. 12). For event SS6, we restore the stratigraphy in the east wall of trench 1. For events SS3 to SS5, we perform similar restoration of the stratigraphy mostly in the west wall, because the deformation shown in this wall includes less warping than in the east wall, and thus requires less "subjective" judgment in the reconstruction. Two assumptions are used in the restoration. First, the ground surface before each event was almost flat. Second, the blocks between fault strands mostly underwent translation (offset) and rigid-body rotation. Although nonbrittle warping is not explicitly considered, its existence would be indicated by the residual nonflat shape in the restored strata.

Restoration of the stratigraphy indicates that SS6 caused about 10 cm of down-dropping on the northern side of the fault, and 35 cm at the main fault zone. Shown in Fig. 12b, the triangular block between two faults near meter 5 is down-dropped and tilted clockwise. This produces a top wedge at the main fault zone, which is subsequently filled up by unit 15. The transgressive unit 14 covers the entire fault zone and further smoothes the topography. Reconstruction of the upper surface of unit 14 before and after event SS5 (Fig. 12d) indicates that the rupture produced a graben at the main fault zone that was down-dropped about 27 cm. The graben was filled later by unit 13. The reconstruction of the top of unit 7 before and after event SS4 (Fig. 12e and f) indicates that the fault breaks of this event have overall normal components of slip, with the north side down by 17 cm. The deformation is mainly in the form of abrupt offsets at faults, because the strata do not show obvious tilting or warping. The comparison between panels g and h of the upper surface of unit 5 shows that the northern side down-dropped another 45 cm due to event SS3. Unlike during event SS4, however, the strata in the vicinity of the main fault zone were deformed by rotation and warping, suggesting that event SS3 was likely bigger than SS4.

Figure 13 further summarizes the difference in amounts of offset during events SS3 and SS4 using a common marker line. Initially, the top of unit 7 was flat, then it was deformed incrementally as it experienced more earthquakes. Overall, event SS3 has a 2.5 times larger vertical offset at the fault than SS4, although there is a similar amount of down-dropping on the north side in the "far field."

Comparison with Previous Paleoseismic Investigations

As described earlier, a paleoseismic investigation was previously conducted at a site ~13 km west of our Songshan site (Fig. 2). Only four events were found to have occurred during the Holocene period, two events between 1675 ± 45 to 1696 ± 50 years B.P. and 4578 ± 60 to 4800 ± 400 years B.P., and another two events between 4578 ±60 to 4800 ± 400 and 9098 ± 76 years B.P., respectively (uncalibrated ages; Liu *et al.*, 1998). Based on the evidence described by Liu *et al.* (1998), it is likely that they uncovered evidence for only a minimum number of earthquakes. Their excavation was located across a cumulative pressure ridge on the lowest terrace of the Heima Zhuang He (Fig. 2), about 4 m above the river bed where little sedimentation occurred between events. Instead, they relied on thin layers of colluvium to separate events because there had been no substantial fluvial deposition since the abandonment of the terrace, probably a few thousand years ago. Depositional hiatus will be cause for events not being recorded or recognized in paleoseismic trenches. In addition, using solely colluvial wedges to differentiate events is problematic in a strike-slip setting (Weldon *et al.*, 1996), especially along a "mole track" type of surface break, with small and variable scarp heights. Thus, it is plausible that several of the recent events we see in the past 3500–3900 years at the current study site were not recognized by Liu *et al.* (1998). We cannot completely rule out the possibility that their site is on one of the two branches (Figs. 1 and 2), thus may miss the rupture on the southern branch. Regardless, it is also possible that the two events they identified between 1675 ± 45 to 1696 ± 50 years B.P. and 4578 ± 60 to 4800 ± 400 years B.P. correspond to either our events SS4 and SS5 or SS5 and SS6, but data are insufficient to prove or disprove this.

Comparison with Historical Seismicity in the Region

The region, which was called Liangzhou before the 1900s, encompasses a variably large territory of western Gansu and eastern Qinghai provinces. Wuwei (Fig. 1), the capital of Liangzhou, is about 120 km northwest of our trench site. The first record of an earthquake dates back to 193 B.C. Table 3 summarizes known historical earthquakes in the broad region since 0 A.D. (Working Group on Historical Earthquake Compilation, Academic Sinica, 1965; Gu *et al.*, 1989).

Searching for accurate dates of our older surface-faulting earthquakes in regional historical accounts may be

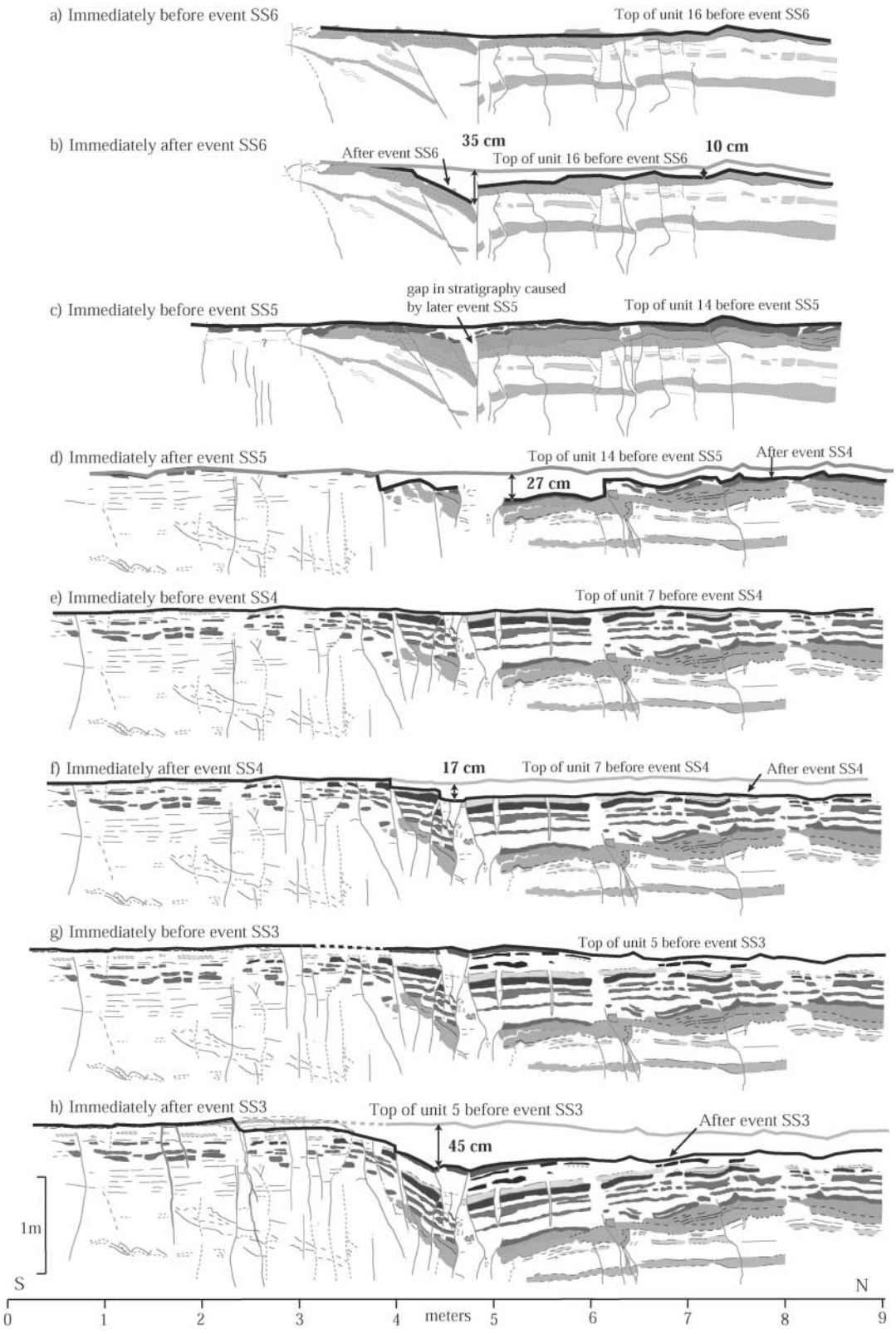

Figure 12. Possible restoration of stratigraphy in trench 1 showing deformation associated with events SS6 to SS3. Panels are arranged to show proposed stratigraphy and ground surface immediately before and after each earthquake is shown. Fault strands activated during each event are highlighted in red. Color coding is according to Figure 6. Panels a to c show the restoration of stratigraphy in the east wall, whereas panels d through h show that in the west wall.

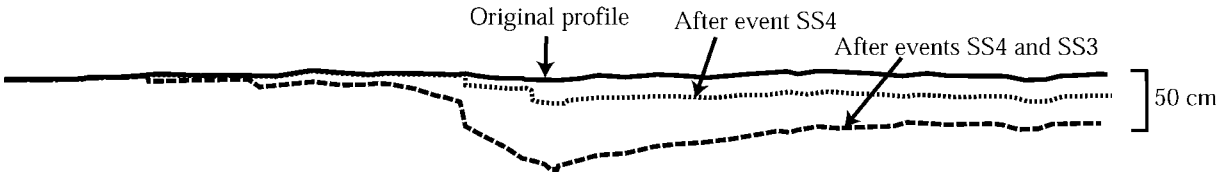

Figure 13. Comparison of amounts of vertical deformation associated with events SS3 and SS4, using the top profile of unit 7 in west wall as the reference line. Event SS3 produced more tilting and warping of strata in the vicinity of the main fault zone than SS4 did.

Table 3
Historical Earthquakes Felt or Caused Damages in Liangzhou (Wuwei)*

Dates of Earthquakes (A.D.)†	Descriptions	Significance of the Earthquake
July 161	Earthquake in Liangzhou	
October 143	Felt in large area including Wuwei, Lingwu (~280 km east of Wuwei), west to Zhangye, south to Wudu (~550 km south-southeast of Wuwei). Mountains rip apart, cities wrecked, people killed; 180 shocks happened from October to the next January.	Large area affected, epicenter uncertain
September 361	Earthquake in Liangzhou.	
26 May 362	Earthquake in Liangzhou.	
March 366	Earthquake in Liangzhou, spring emerged.	
8 August 374 (reports of 371 A.D. may be erroneous)	In Liangzhou: earthquakes continuously occurred in multiple years. Landslides; springs emerged. In Xining: rocks cascade the mountain in Tulou (northwest of Xining city). Ten shocks occurred in 50 days. Gu *et al.* (1989) thought that the quake reported in Liangzhou and Xining should be the same earthquake.	Could be on the western Haiyuan fault
30 August 506	A thundering earthquake struck Liangzhou (Wuwei); city gate collapsed.	
14 January 575 (could be reported as in 573 or January 574)	Earthquakes continuously occurred in Liangzhou in multiple years. City wall destroyed. The ground cracked and springs emerged.	A 1927 Gulang earthquake-type thrust event?
27 November 756	Zhangye and Jiuquan were worst hit. Ground sank or cracked. Audible sound could be heard in Liangzhou.	Distant earthquake, west of Wuwei
Winter 1092 (1 November 1092)	Earth shocked violently, towers tilted. Also felt in Lanzhou.	Could be 1920 M >8 Haiyuan earthquake type on the Haiyuan fault
18 December 1380	Earthquake in Hezhou (Linxia) and Liangzhou (vague)	
28 January 1381 and 21 April 1381	Earthquake in Liangzhou	
21 September 1471 and 21 October 1471	Earthquake with thunders in Liangzhou	
13 May 1477	Yingchuan earthquake	Distant earthquake to the northeast in the Yingchuan graben
7 December 1514	Earthquake at Wuwei, Yongcang (~65 km northwest of Wuwei) and Yongdeng (~140 km southeast of Wuwei) with thunders.	Earthquake on the Haiyuan fault, local to our site?
7 January 1558	Earthquake and thunders in Wuwei and other places	
9 October 1587	Yongcang (~65 km northwest of Wuwei) earthquake, sound heard in Wuwei.	
1665	Top of a temple in western Wuwei fell.	On a thrust fault northwest of our site?
14 October 1709	Giant earthquake, worst hit in Zhongwei. Many accounts of damage in large area, felt in towns 900 km east of Zhongwei.	Earthquake occurred on the Tianjin Shan thrust fault north of the Haiyuan fault

*See locations of most towns in Figure 1.

†Earthquakes that may correlate with surface-faulting events on the Haiyuan fault exposed at the Songshan trench site are shown in **bold** and discussed further in the text.

Data sources: Working group on historical earthquake compilation, Academic Sinica (1965), and Gu *et al.* (1989).

biased for several reasons (see also Gaudemer *et al.*, 1995). First, accounts of earthquakes are in general brief, especially in the early history of the area (e.g., before 1600 A.D.). For example, the 1125 A.D., $M > 7$, Lanzhou earthquake (a population center larger than or comparable to Wuwei), is described in less than 50 words. Such brief earthquake accounts in such a vast region make it hard to determine which fault might be responsible for a specific event. Second, for a long time this region was located at the frontier of Han culture, with northwest nomadic tribes making it more unstable than the interior of the Han empires, which certainly affected the completeness of the historical record. Third, population centers in the region (e.g., Wuwei) are often located on alluvial plains outside the high mountain ranges, thus at some distance from active faults with high slip rates (Fig. 1). Even the shaking effect from a great earthquake on the Haiyuan fault might be damped considerably because of the large distance. In short, historical accounts in such a sparsely populated region will not permit us to distinguish moderate local earthquakes from large distant ones. In addition, the uncertainty in ages of paleoseismic events in the Songshan trench using bounds on ^{14}C samples in the stratigraphy further compounds the problem. For example, given the 0–410 A.D. range of our trench event SS4, multiple possible matches occur, including July 161 A.D., October 143 A.D., September 361 A.D., May 362 A.D., March 366 A.D., and 8 August 374 A.D (Table 3). The brief historical account of each of these earthquakes makes it impossible to be sure which among them correlates with event SS4.

Despite such difficulties, one may still make plausible attempts at reconciling historical accounts (Table 2) with our paleoseismic events. We reason that a large earthquake on the Haiyuan fault would be felt in a large area. The largest towns in the region besides Wuwei, in ancient times as well as now, are Xining and Lanzhou located to the south of the Haiyuan fault (Fig. 1). Xining and Lanzhou are located 80 km and 90 km, respectively, from the nearest approach to the fault. For both cities, this is the closest and most active seismogenic fault. An earthquake felt in both Wuwei and Xining or Lanzhou would thus be a good candidate for one of our paleoseismic events.

In keeping with this line of reasoning, the best candidates for event SS4, which occurred during 0–410 A.D., are the October 143 A.D. and 8 August 374 A.D. earthquakes. If event SS3 occurred shortly after 890–1000 A.D., it could be the winter 1092 A.D. earthquake. This earthquake was felt both in Lanzhou and Wuwei, and hence was a large event. Furthermore, one paleoseismic investigation (Ran *et al.*, 1997), at a site 130 km east of Songshan (Fig. 14), concluded that the penultimate event prior to the 1920 great earthquake occurred sometime after 540 ± 65 B.P. (^{14}C) and before 1470 ± 120 yr (TL dating). It could be correlated with event SS3 and the 1092 A.D. historical earthquake. For event SS2, which occurred sometime during 1440–1640 A.D., the best candidate would be the 7 December 1514 earthquake. This earthquake was felt in Wuwei, Yongcang, and Yundeng, cities close to the Haiyuan fault, but not in places farther away. Therefore, it was probably a relatively local event. This is supported by trench evidence that event SS2 caused smaller disturbance and offset than events SS3 through SS6.

Based on the preceding discussion, we show a preliminary scenario of earthquake ruptures for the four youngest events exposed in the Songshan trenches (Fig. 14). Events SS4 and SS3 would have been large earthquakes, with rupture lengths over 200 km, comparable to the 1920 Haiyuan (M 8) earthquake. If event SS2 had a rupture of about 60 km, then it could be a M 7+ event (Wells and Coppersmith, 1994), either on the Maomaoshan segment of the Haiyuan fault, or possibly on the South Maomaoshan branch of the Haiyuan fault (Gaudemer *et al.*, 1995). This portion of the fault has the required length between the Tianzhu pull-apart basin and the Songshan junction. Figure 14 also depicts the ruptures of three large historical earthquakes in 1709, 1920, and 1927 in the region.

Implications for the Slip Rate on the Western Haiyuan Fault

Lasserre *et al.* (1999) inferred that the range of slip per event was between 8 and 16 m and suggested that 10 m was the smallest small-scale geomorphic offset recognizable in this reach of the fault. Event SS2 is characterized by only minor fractures and fissures with little or no vertical offset, but we cannot exclude that it might have had a horizontal offset of up to a few tens of centimeters (≤1 m). For example, the over-100-km-long rupture of the M ~7.5 earthquake that occurred on 8 December 1812 A.D. along the San Andreas fault (Jacoby *et al.*, 1988) was manifested in trenches at the Wrightwood site by only open fissures and an unconformity (Fumal *et al.*, 1993, 2002). Yet, at this site it had more than one meter of horizontal offset (Weldon *et al.*, 2004). Thus, by comparison, event SS2 at the Songshan site could represent a significant earthquake (M ~7?). It seems possible that the 10-m smallest geomorphic offset estimate of Lasserre *et al.* (1999) may represent a combination of event SS2 and a previous larger-offset event. Event SS3 most likely represents a large, several-meter-offset earthquake. If we further assume that event SS2 had an offset of <1 m, then event SS3 might have had an offset of about 10 m. Event SS3 might have had a greater horizontal offset than event SS4, given the larger vertical offset visible in the trench. Both events SS3 and SS4 might have had offsets similar to the 1920 Haiyuan earthquake (maximum slip, 10–11 m) (Zhang *et al.*, 1987), and therefore comparable magnitudes (M 8) (see also rupture lengths on Figs. 1 and 14).

Inferring the horizontal offsets of events SS3 and SS4 to be 10 ± 2 m, a crude slip-time diagram would be more consistent with the slip rate of 8–16 mm/yr found by Lasserre *et al.* (1999) and Gaudemer *et al.* (1995) during the past 2000 years (Fig. 15), than with that of 5 mm/yr inferred by He *et al.* (1994, 1996) and Yuan *et al.* (1998). An ide-

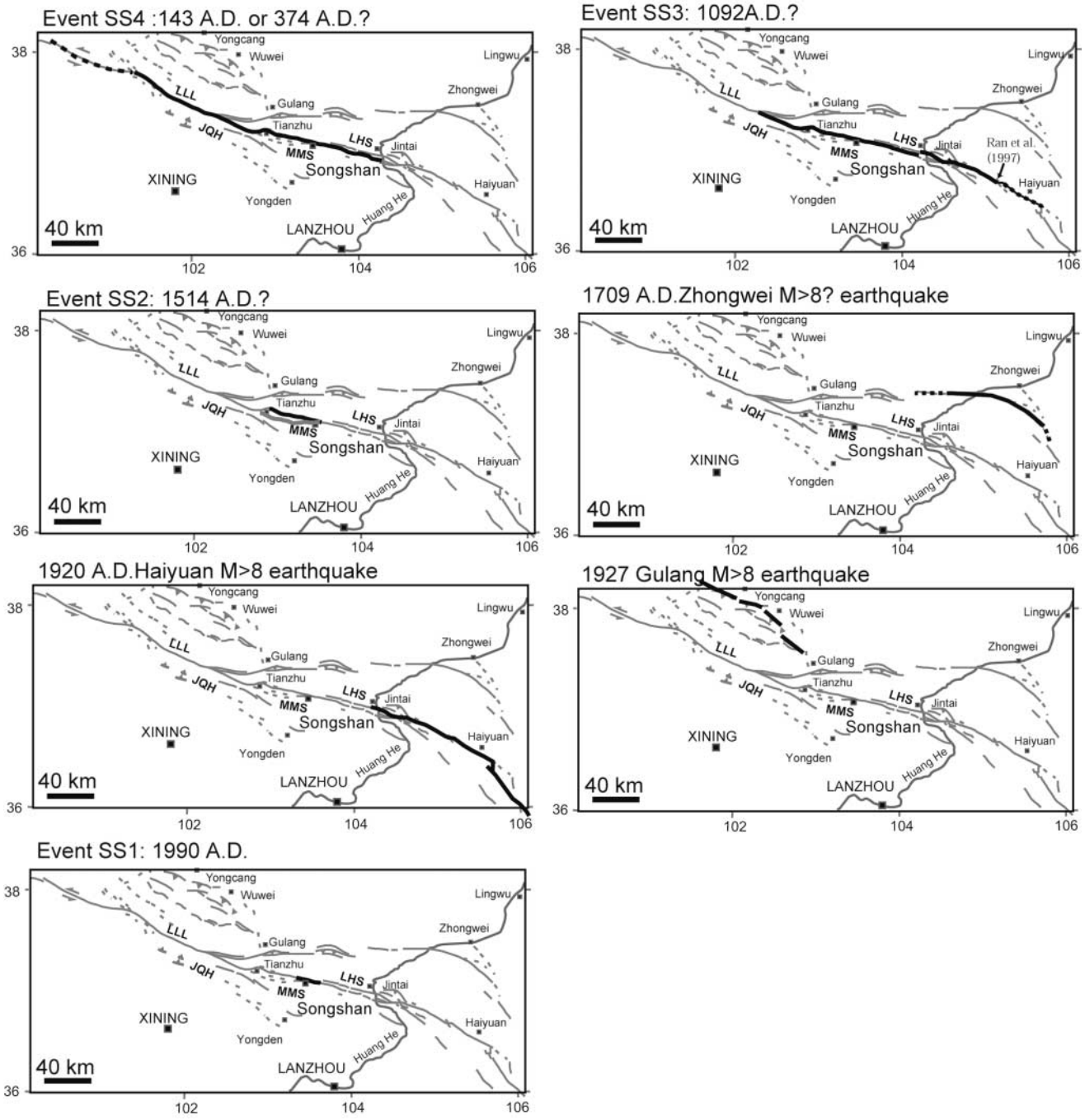

Figure 14. Hypothesized rupture extents (bold dark lines) of the youngest four events exposed at the Songshan site. Events SS3 and SS4 were likely large events similar to the 1920 M >8 Haiyuan earthquake. The smaller event SS2 was located either on the main trace of Haiyuan fault, or the continuation from a secondary branch to the south (shown as a bold-gray line). Also shown are the ruptures associated with three large regional historical earthquakes in 1709, 1920, and 1927.

alized projection of the occurrence times of events SS3 and SS4 also implies that an earthquake may be pending, and now this stretch of the fault is close to the end of a seismic cycle. If the preliminary low GPS rate on the Haiyuan fault is real, the long time since the last large event seems to lend support to the suggestion that geodetic measurements might underestimate slip rate if the fault is late in its earthquake cycle (Chevalier *et al.*, 2005).

Clearly, however, without rigorous measurements of slip per event for the earthquakes exposed in the Songshan trenches, the slip-rate estimation shown in Figure 15 should be considered, at best, not contradictory with the slip rate

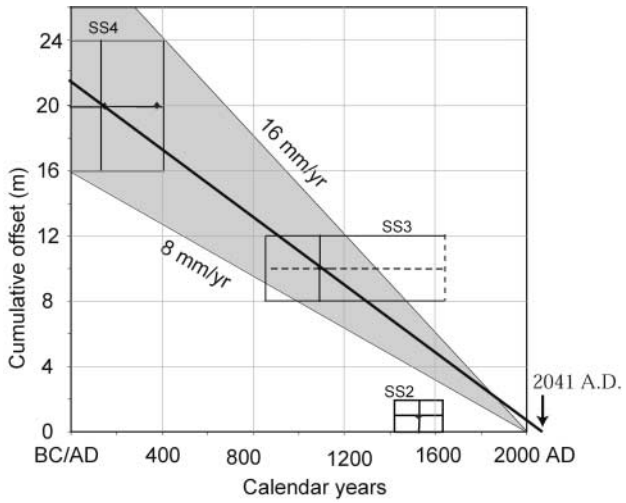

Figure 15. Slip-time function during the past 2000 years. Events SS4 and SS3 are assumed to have 10 ± 2 m offsets. The best fit gives the apparent slip rate of 8–16 mm/yr. The dimensions of boxes designate the errors in age and offset estimates.

inferred from cumulative horizontal offsets at dated terrace sites. Our study is merely a first step toward understanding the long-term seismic behavior of the western Haiyuan fault. As pointed out by Weldon *et al.* (1996) and demonstrated (Liu *et al.*, 2004; Liu-Zeng *et al.*, 2006), a site adequate for dating paleoearthquakes may not be an ideal site for measuring slip per events, and vice versa. Future work to determine the slip associated with each event at sites nearby will provide much needed critical information about the earthquake history on this section of the Haiyuan fault.

Summary

Two trenches were excavated at a stepover on the Haiyuan fault, north of Songshan (37.1° N, 103.5° E). They exposed stratigraphic evidence for six paleoearthquakes, events SS1, SS2, SS3, SS4, SS5, and SS6 from youngest to oldest, in the upper 3 m of sediments. Based on charcoal samples, the earthquakes occurred after 1530–1888 B.C. or in the past 3500–3900 years. Samples within the uppermost 2 m of sediments further constrain the youngest four events to have occurred in the past ~2000 years since 0–230 A.D. The youngest event (SS1) ruptured the ground surface with only one or two tensile crack in one trench. It is likely correlated with the local 1990 M_w 5.8 earthquake. Events SS2, SS3, and SS4 occurred sometime during the periods 1440–1640 A.D., shortly after 890–1000 A.D., and 0–410 A.D., respectively. The trenches do not provide information about horizontal slip during these events. However, events SS3 to SS6, which caused a few tens of centimeters of vertical offset and prominent tilting of depositional layers, appear to be larger events. We tentatively associate events SS2, SS3, and SS4, respectively, to the 1514 A.D., 1092 A.D., and 143 or 374 A.D. historical earthquakes in the region. If we take the estimation of 10 ± 2 m of slip per large event (Lasserre *et al.*, 1999), the millennial recurrence time of large events does not contradict the 12 ± 14 mm/yr average slip rate found by Gaudemer *et al.* (1995) and Lasserre *et al.* (1999). Clearly, a more robust slip-rate estimate depends on more rigorous determination of slip per individual earthquake.

Acknowledgments

This collaborative work was partly funded by Association Franco-Chinoise pour la Recherché Scientifique et Technique (Y.K. and X.X.), by the French Embassy in China, the Chinese National Science Foundation (Project no. 4047 4037), and a Chateaubriand Fellowship from the French Foreign Affair Ministry (J.L.-Z.). Part of the AMS ^{14}C dating was processed at the French National Laboratory LMC14. We thank staff at Lanzhou Institute of Seismology, China Earthquake Administration, and two drivers (Xianglong Wang and Cheng Fu) for logistic arrangements and A.-C. Morillon for Figure 3. S. Olig and M. Hemphill-Haley provided us with a very helpful review that improved this manuscript. This is IPGP contribution no. 2152.

References

Avouac, J., and P. Tapponnier (1993). Kinematic model of active deformation in central Asia, *Geophys. Res. Lett.* **20,** 895–898.

Barka, A., H. S. Akyuz, E. Altunel, G. Sunal, Z. Cakir, A. Dikbas, B. Yerli, R. Armijo, B. Meyer, J. B. de Chabalier, T. Rockwell, J. R. Dolan, R. Hartleb, T. Dawson, S. Christofferson, A. Tucker, T. Fumal, R. Langridge, H. Stenner, W. Lettis, J. Bachhuber, and W. Page (2002). The surface rupture and slip distribution of the 17 August 1999 Izmit earthquake (M 7.4), North Anatolian fault, *Bull. Seism. Soc. Am.* **92,** 43–60.

Barka, A. A., R. C. Buckman, and P. L. Hancock (1992). The North Anatolian fault zone, *Ann. Tecton.* **6** (Suppl.), 164–195.

Bendick, R., R. Bilham, J. T. Freymueller, K. Larson, and G. Yin (2000). Geodetic evidence for a low slip rate in the Altyn Tagh fault, *Nature* **404,** 69–72.

Blong, R. J., and R. Gillespie (1978). Fluvially trasported charcoal gives erroneous ^{14}C ages for recent deposits, *Nature* **271,** 739–741.

Burchfiel, B. C., Z. Peizhen, W. Yipeng, Z. Weiqi, S. Fangmin, D. Qidong, P. Molnar, and L. Royden (1991). Geology of the Haiyuan Zone, Ningxia-Hui Autonomous Region, China, and its relation to the evolution of the northeastern margin of the Tibetan Plateau, *Tectonics* **10,** 1091–1110.

Chen, Q., J. Freymueller, Q. Wang, Z. Yang, C. Xu, and J. Liu (2004). A deforming block model for the present-day tectonics of Tibet, *J. Geophys. Res.* **109,** B01403, doi 01410.01029/02002JB002151.

Chevalier, M. L., F. J. Ryerson, P. Tapponnier, R. C. Finkel, J. v. d. Woerd, H. Li, and Q. Liu (2005). Slip-rate measurements on the Karakorum fault may imply secular variations in fault motion, *Science* **307,** 411–414.

Committee for Chinese Earthquake Bulletin (1990). The October 20, 1990 Ms 6.2 Tianzhu—Jintai, Gansu earthquake, in *Chinese Earthquake Yearly Bulletin, 1990*, Seismological Publishing House, Beijing, 167–171.

Deng, Q., F. Song, S. Zhu, Y. Wang, W. Zhang, D. Jiao, B. C. Burchfiel, P. Molnar, L. Royden, and P. Zhang (1986). Variations in the geometry and amount of slip on the Haiyuan (Nanxihaushan) fault zone, China, and the surface rupture of the 1920 Haiyuan earthquake, in *Earthquake Source Mechanics*, S. Das, J. Boatwright, and C. H. Scholz (Editors), American Geophysical Monograph 37, 169–182.

Ding, G., J. Chen, Q. Tian, X. Shen, C. Xing, and K. Wei (2004). Active faults and magnitudes of left-lateral displacement along the northern margin of the Tibetan Plateau, *Tectonophysics* **380,** 243–260.

Dixon, T. H., M. M. Miller, F. Farina, H. Wang, and D. Johnson (2000). Present-day motion of the Sierra Nevada block and some tectonic implications for the Basin and Range province, North America Cordillera, *Tectonics* **19,** 1–24.

Dixon, T. H., E. Norabuena, and L. Hotaling (2003). Paleoseismology and Global Positioning System: earthquake-cycle effects and geodetic versus geologic fault slip rates in the Eastern California shear zone, *Geology* **31,** 55–58.

Dokka, R. K., and C. J. Travis (1990). Late Cenozoic strike-slip faulting in the Mojave Desert, California, *Tectonics* **9,** 311–340.

England, P., and G. Houseman (1986). Finite strain calculations of continental deformation, 2. Comparison with the India-Asia collision zone, *J. Geophys. Res.* **91,** 3664–3676.

Fumal, T. E., S. K. Pezzopane, R. J. Weldon, and D. P. Schwartz (1993). A 100-year average recurrence interval for the San Andreas fault at Wrightwood, California, *Science* **259,** 199–203.

Fumal, T. E., R. J. Weldon, G. P. Biasi, T. E. Dawson, G. G. Seitz, W. T. Frost, and D. P. Schwartz (2002). Evidence for large earthquakes on the San Andreas fault at the Wrightwood, California paleoseismic site: A.D. 500 to present, *Bull. Seism. Soc. Am.* **92,** 2726–2760.

Gansu Bureau of China Earthquake Administration and Lanzhou Institute of Seismology, China Earthquake Administration (1990). Field report of the 1990 Tianzhu-Jintai earthquake, Gansu Province.

Gaudemer, Y., P. Tapponnier, B. Meyer, G. Peltzer, S. Guo, Z. Chen, H. Dai, and I. Cifuentes (1995). Partitioning crustal slip between linked, active faults in the eastern Qilian Shan, and evidence for a major seismic gap, the "Tianzhu Gap", on the western Haiyuan Fault, Gansu (China), *Geophys. J. Int.* **120,** 599–645.

Gaudemer, Y., P. Tapponnier, and D. Turcotte (1989). River offsets across active strike-slip faults, *Ann. Tecton.* **3,** 55–76.

Grant, L. B., and K. Sieh (1993). Stratigraphic evidence for seven meters of dextral slip on the San Andreas Fault during the 1857 earthquake in the Carrizo Plain, *Bull. Seism. Soc. Am.* **83,** 619–635.

Grant, L. B., and K. Sieh (1994). Paleoseismic evidence of clustered earthquakes on the San Andreas Fault in the Carrizo Plain, California, *J. Geophys. Res.* **99,** 6819–6841.

Gu, G., T. Lin, and Z. Shi (1989). *Catalogue of Chinese earthquakes (1831 BC–1969 AD)*, Science Press, Beijing, China, 872 pp.

He, W., B. Liu, T. Lu, D. Yuan, and X. Liu (1996). The late Quaternary activity of the Maomaoshan fault zone, in *Research on Active Fault Series 5*, Q. Deng, Y. Wang, and P. Zhang (Editors), Seismological Press, Beijing, China, 63–77 (in Chinese with English abstract).

He, W., B. Liu, T. Lu, D. Yuan, J. Liu, and X. Liu (1994). Study on the segmentation of Laohushan fault zone, *Northwestern Seism. J.* **16,** 66–72 (in Chinese with English abstract).

Houseman, G., and P. England (1993). Crustal thickening versus lateral expulsion in the Indian—Asian continental collision, *J. Geophys. Res.* **98,** 12,233–12,249.

Hubert-Ferrari, A., G. King, I. Manighetti, R. Armijo, B. Meyer, and P. Tapponnier (2003). Long-term elasticity in the continental lithosphere; modeling the Aden Ridge propagation and the Anatolian extrusion process, *Geophys. J. Int.* **153,** 111–132.

Institute of Geology, China Earthquake Administration and Ninxia Bureau of China Earthquake Administration (1990). *Active Haiyuan Fault Zone Monograph*, Special Publications on Active Fault Studies in China, Seismological Publishing House, Beijing, 286 pp.

Jacoby, G. C., P. R. Sheppard, and K. E. Sieh (1988). Irregular recurrence of large earthquakes along the San Andreas Fault; evidence from trees, *Science* **241,** 196–199.

Lasserre, C. (2000). Fonctionnement sismique, cinématique et histoire géologique de la faille d'Haiyuan, *Ph.D. Thesis*, Université Paris **7,** 244 pp.

Lasserre, C., P. H. Morel, Y. Gaudemer, P. Tapponnier, F. J. Ryerson, G. C. P. King, F. Metivier, M. Kasser, M. Kashgarian, B. Liu, T. Lu, and D. Yuan (1999). Postglacial left slip rate and past occurrence of $M >$ or $= 8$ earthquakes on the western Haiyuan Fault, Gansu, China, *J. Geophys. Res.* **104,** 17,633–17,652.

Lasserre, C., B. Bukchin, P. Bernard, P. Tapponnier, Y. Gaudemer, A. Mostinsky, and D. Rong (2001). Source parameters and tectonic origin of the 1996 June 1 Tianzhu (M (sub w) = 5.2) and 1995 July 21 Yongden (M (sub w) = 5.6) earthquakes near the Haiyuan Fault (Gansu, China), *Geophys. J. Int.* **144,** 206–220.

Lasserre, C., Y. Gaudemer, P. Tapponnier, A. S. Meriaux, J. Van der Woerd, D. Yuan, F. J. Ryerson, R. C. Finkel, and M. W. Caffee (2002). Fast late Pleistocene slip rate on the Leng Long Ling Segment of the Haiyuan Fault, Qinghai, China, *J. Geophys. Res.* **107,** B11, 2276, doi 10.1029/2000JB000060.

Liu, B., W. He, X. Liu, and D. Yuan (1998). Study on the trench of paleoearthquake in compressive ridge, in *Research on Active Fault Series 6*, Q. Deng, Y. Wang, and P. Zhang (Editors), Seismological Press, Beijing, China, 56–65 (in Chinese with English abstract).

Liu, J., Y. Klinger, K. Sieh, and C. Rubin (2004). Six similar sequential ruptures of the San Andreas fault, Carrizo Plain, California, *Geology* **32,** 649–652, doi 10.1130/G20478.1.

Liu-Zeng, J., Y. Klinger, K. Sieh, C. Rubin, and G. Seitz (2006). Serial ruptures of the San Andreas Fault, Carrizo Plain, California, revealed by three-dimensional excavations, *J. Geophys. Res.* **111,** B02306, doi 10.1029/2004JB003601.

Mériaux, A.-S., F. J. Ryerson, P. Tapponnier, J. Van der Woerd, R. C. Finkel, X. Xu, Z. Xu, and M. W. Caffee (2004). Rapid slip along the central Altyn Tagh fault: morphochronologic evidence from Cherchen He and Sulamu Tagh, *J. Geophys. Res.* **109,** B06401, doi 06410.01029/02003JB002558.

Mériaux, A.-S., P. Tapponnier, F. J. Ryerson, X. Xu, G. King, J. V. d. Woerd, R. C. Finkel, H. Li, M. W. Caffee, Z. Xu, and W. Chen (2005). The Aksay segment of the northern Altyn Tagh fault: tectonic geomorphology, landscape evolution, and Holocene slip rate, *J. Geophys. Res.* **110,** B04404 doi 04410.01029/02004JB003210.

Miller, M. M., D. J. Johnson, T. H. Dixon, and R. K. Dokka (2001). Refined kinematics of the Eastern California shear zone from GPS observations, *J. Geophys. Res. B Solid Earth Planets* **106,** 2245–2264.

Min, W., P. Zhang, and Q. Deng (2000). Preliminary study of regional paleoseismic behavior, *Acta Seism. Sinica* **22,** 163–170 (in Chinese with English abstract).

Nelson, A. R. (1992). Discordant ^{14}C ages buried tidal-marsh soils in the Cascadia subduction zone, southern Oregon coast, *Quat. Res.* **38,** 74–90.

Oskin, M., and A. Iriondo (2004). Large-magnitude transient strain accumulation on the Blackwater Fault, Eastern California shear zone, *Geology* **32,** 313–316.

Peltzer, G., and P. Tapponnier (1988). Formation and evolution of strike-slip faults, rifts, and basins during the India-Asia collision: an experimental approach, *J. Geophys. Res.* **93,** 15,085–15,117.

Peltzer, G., F. Crampé, S. Hensley, and P. Rosen (2001). Transient strain accumulation and fault interaction in the Eastern California shear zone, *Geology* **29,** 975–978.

Peltzer, G., P. Tapponnier, Y. Gaudemer, B. Meyer, S. Guo, K. Yin, Z. Chen, and H. Dai (1988). Offsets of late Quaternary morphology, rate of slip, and recurrence of large earthquakes on the Chang Ma Fault (Gansu, China), *J. Geophys. Res.* **93,** 7793–7812.

Perfettini, H., and J. P. Avouac (2004). Stress transfer and strain rate variations during the seismic cycle, *J. Geophys. Res.* **109,** B06402, doi 06410.01029/02003JB002917.

Ramsey, C. B. (2000). OxCal Program Ver. 3.5, Radiocarbon Accelerator4 Unit, University of Oxford, U.K., http://www.rlaha.ox.ac.uk/ (last accessed December 2006).

Ran, R., R. Duan, Q. Deng, D. Jiao, and W. Min (1997). 3-D trench excavation and paleoseismology at Gaowanzi of the Haiyuan fault, *Seism. Geol.* **19,** 97–107 (in Chinese with English abstract).

Rockwell, T. K., D. L. Lamar, R. S. McElwain, and D. E. Millman (1986). Recurrent late Holocene faulting on the Glen Ivy North Strand of the Elsinore fault at Glen Ivy Marsh, in *Neotectonics and Faulting in Southern California*, P. Ehlig (Editor), Geol. Soc. Am. Fieldtrip

Guidebook for the Cordilleran Section Meeting in Los Angeles, 167–176.

Rockwell, T. K., S. Lindvall, M. Herzberg, D. Murbach, T. Dawson, and G. Berger (2000). Paleoseismology of the Johnson Valley, Kickapoo, and Homestead Valley faults; clustering of earthquakes in the eastern California shear zone, *Bull. Seism. Soc. Am.* **90,** 1200–1236.

Rubin, C. M., and K. Sieh (1997). Long dormancy, low slip rate, and similar slip-per-event for the Emerson Fault, eastern California shear zone, *J. Geophys. Res. B Solid Earth Planets* **102,** 319–315.

Segall, P. (2002). Integrating geologic and geodetic estimates of slip rate on the San Andreas fault system, *Int. Geol. Rev.* **44,** 62–82.

Shen, Z.-K., M. Wang, Y. Li, D. D. Jackson, A. Yin, D. Dong, and P. Fang (2001). Crustal deformation along the Altyn Tagh Fault system, western from GPS, *J. Geophys. Res., B Solid Earth Planets* **106,** 30,607–30,621.

Sieh, K. (1978). Prehistoric large earthquakes produced by slip on the San Andreas fault at Pallett Creek, California, *J. Geophys. Res. B Solid Earth Planets* **83,** 3907–3939.

Stein, R., A. Barka, and J. H. Dieterich (1997). Progressive failure on the North Anatolian fault since 1939 by earthquake stress triggering, *Geophys. J. Int.* **128,** 594–604.

Stuiver, M., P. J. Reimer, E. Bard, J. W. Beck, G. S. Burr, K. A. Hughen, B. Kromer, G. McCormac, J. van der Plicht, and M. Spurk (1998). INTCAL98 radiocarbon age calibration, 24,000-0 cal BP, *Radiocarbon* **40,** 1041–1083.

Sykes, L. R., J. B. Kisslinger, L. S. House, J. N. Davies, and K. H. Jacob (1981). Rupture zones and repeat times of great earthquakes along the Alaska-Aleutian Arc, 1784–1980, in *Earthquake Prediction: An International Review, Maurice Ewing Series 4*, D. W. Simpson and P. G. Richards (Editors), America Geophysical Union, Washington, D.C., 73–79.

Tapponnier, P., X. Zhiqin, F. Roger, B. Meyer, N. Arnaud, G. Wittlinger, and Y. Jingsui (2001). Oblique stepwise rise and growth of the Tibet plateau, *Science* **294,** 1671–1677.

Van der Woerd, J., F. J. Ryerson, P. Tapponnier, A. S. Meriaux, Y. Gaudemer, B. Meyer, R. C. Finkel, M. W. Caffee, G. Zhao, and Z. Xu (2000). Uniform slip-rate along the Kunlun Fault; implications for seismic behaviour and large-scale tectonics, *Geophys. Res. Lett.* **27,** 2353–2356.

Van der Woerd, J., P. Tapponnier, F. J. Ryerson, A.-S. Meriaux, B. Meyer, Y. Gaudemer, R. C. Finkel, M. W. Caffee, G. Zhao, and Z. Xu (2002). Uniform postglacial slip-rate along the central 600 km of the Kunlun Fault (Tibet), from (super 26) Al, (super 10) Be, (super 14) C dating of riser offsets, and climatic origin of the regional morphology, *Geophys. J. Int.* **148,** 356–388.

Vaughan, P. R., K. M. Thorup, and T. K. Rockwell (1999). Paleoseismology of the Elsinore Fault at Agua Tibia Mountain, southern California, *Bull. Seism. Soc. Am.* **89,** 1447–1457.

Wallace, K., G. Yin, and R. Bilham (2005). Inescapable low slip on the Altyn Tagh fault, *Geophys. Res. Lett.* **31,** L09613, doi 10.1029/2004GL019724.

Wang, Q., P. Z. Zhang, J. T. Freymueller, R. Bilhan, K. M. Larson, X. Lai, X. Z. You, Z. J. Niu, J. C. Wu, Y. X. Li, J. N. Liu, Z. Q. Yang, and Q. Z. Chen (2001). Present-day crustal deformation in China constrained by global positioning system measurements, *Science* **294,** 574–577.

Weldon, R., P. McCalpin, and T. K. Rockwell (1996). Paleoseismology of strike-slip tectonic environments, in *Paleoseismology*, J. McCalpin (Editor), Academic Press, San Diego, 271–329.

Weldon, R., K. Scharer, T. Fumal, and G. Biasi (2004). Wrightwood and the earthquake cycle; what a long recurrence record tells us about how faults work, *GSA Today* **14,** 4–10.

Wells, D. L., and K. J. Coppersmith (1994). New empirical relationships among magnitude, rupture length, rupture width, rupture area, and surface displacement, *Bull. Seism. Soc. Am.* **84,** 974–1002.

Working group on the Altyn Tagh active fault (1992). *Active Altun Fault Zone Monograph*, Special Publications on Active Fault Studies in China, Seismological Publishing House, Beijing, 319 pp.

Working group on historical earthquake compilation, Academic Sinica (1956). Catalogue of earthquake accounts in Gansu Province, in *Catalogue of Chinese Earthquakes*, Science Press, Beijing, 440–562.

Xiang, H., S. Guo, B. Zhang, W. Zhang, Y. Ikeda, and H. He (1998). Active features of the eastern Liupanshan piedmont reverse fault zone since late Quaternary, *Seism. Geol.* **20,** 321–327 (in Chinese with English abstract).

Yeats, R., K. Sieh, and C. Allen (1997). *The Geology of Earthquakes*, Oxford University Press, New York, 568 pp.

Yuan, D., B. Liu, T. Lu, W. He, X. Liu, and W. Gan (1998). Study on the segmentation in east segment of the northern Qilianshan fault zone, *Northwestern Seism. J.* **20,** 27–34 (in Chinese with English abstract).

Zhang, P., P. Molnar, B. C. Burchfiel, L. Royden, Y. Wang, Q. Deng, S. Fangmin, Z. Weiqi, J. Decheng, F. Song, W. Zhang, and D. Jiao (1988). Bounds on the Holocene slip rate of the Haiyuan Fault, north-central China, *Quat. Res.* **30,** 151–164.

Zhang, P., P. Molnar, W. Zhang, Q. Deng, Y. Wang, B. C. Burchfiel, F. Song, L. H. Royden, and D. Jiao (1988). Bounds on the average recurrence interval of major earthquakes along the Haiyuan fault in north-central China, *Seism. Res. Lett.* **59,** 81–89.

Zhang, P., Z. Shen, M. Wang, W. Gan, R. Buergmann, P. Molnar, Q. Wang, Z. Niu, J. Sun, J. Wu, H. Sun, and X. You (2004). Continuous deformation of the Tibetan Plateau from Global Positioning System data, *Geology* **32,** 809–812.

Zhang, W., D. Jiao, P. Zhang, P. Molnar, B. C. Burchfiel, Q. Deng, Y. Wang, and F. Song (1987). Displacement along the Haiyuan fault associated with the great 1920 Haiyuan, China, earthquake, *Bull. Seism. Soc. Am.* **77,** 117–131.

Laboratoire de Tectonique
Institut de Physique du Globe de Paris
BP89, 4 place Jussieu
75005 Paris, France
(J.L.-Z., Y.K., P.T.)

Institute of Tibetan Plateau Research
Chinese Academy of Sciences
P.O. Box 2871, 18 Shuang Qing Road
Beijing 100085, China
(J.L.-Z.)

Insitute of Geology
China Earthquake Administration
Beijing 100029, China
(X.X., G.C., W.C.)

Laboratoire de Géologie
Ecole Normale Supérieure
24 Rue Lhomond
75231 Paris Cedex 05, France
(C.L.)

Tianzhu Bureau of Earthquake Administration
92 Tuanjie Road Tianzhu County
Gansu Province 733200, China
(B.Z.)

Manuscript received 9 June 2005.